

AG2S/2-MPA QUANTUM DOTS; CYTOTOXICITY AND CELLULAR
INTERNALIZATION

A THESIS SUBMITTED TO
THE GRADUATE SCHOOL OF NATURAL AND APPLIED SCIENCES
OF
MIDDLE EAST TECHNICAL UNIVERSITY

BY

RENGİN ERDEM

IN PARTIAL FULFILLMENT OF THE REQUIREMENTS
FOR
THE DEGREE OF MASTER OF SCIENCE
IN
BIOTECHNOLOGY

JUNE 2012

Approval of the thesis:

**AG2S/2-MPA QUANTUM DOTS; CYTOCOMPATIBILITY AND
CELLULAR INTERNALIZATION**

submitted by **RENGİN ERDEM** in partial fulfillment of the requirements for the degree of **Master of Science in Biotechnology Department, Middle East Technical University** by,

Prof. Dr. Canan Özgen
Dean, **Graduate School of Natural and Applied Sciences** _____

Prof. Dr. Nesrin Hasırcı
Head of the Department, **Biotechnology** _____

Assist. Prof. Dr. Can Özen
Supervisor, **Department of Biotechnology, METU** _____

Assoc. Prof. Dr. Havva Funda Yağcı Acar
Co-supervisor, **Department of Chemistry, Koç University** _____

Examining Committee Members:

Assoc. Prof. Dr. Mesut Muyan
Biological Sciences Dept., METU _____

Assist. Prof. Dr. Can Özen
Department of Biotechnology, METU _____

Assoc. Prof. Dr. Havva Funda Yağcı Acar
Department of Chemistry, Koç University _____

Dr. Tamay Şeker
Central Laboratory, METU _____

Assoc. Prof. Dr. Dilek Keskin
Department of Engineering Sciences, METU _____

Date: 07.06.2012

I hereby declare that all information in this document has been obtained and presented in accordance with academic rules and ethical conduct. I also declare that, as required by these rules and conduct, I have fully cited and referenced all material and results that are not original to this work.

Name, Last name: Rengin Erdem

Signature:

ABSTRACT

AG₂S/2-MPA QUANTUM DOTS; CYTOTOXICITY AND CELLULAR INTERNALIZATION

Erdem, Rengin

M.Sc., Department of Biotechnology

Supervisor: Assist. Prof. Dr. Can Özen

Co-Supervisor: Assoc. Prof. Dr. Havva Funda Yağcı Acar

June 2012, 67 pages

Quantum dots are fluorescent semiconductor nanocrystals that have unique optical properties such as high quantum yield and photostability. These nanoparticles are superior to organic dyes and fluorescent proteins in many aspects and therefore show great potential for both *in vivo* and *in vitro* imaging and drug delivery applications. However, cytotoxicity is still one of the major problems associated with their biological applications.

The aim of this study is *in vitro* characterization and assessment of biological application potential of a novel silver sulfide quantum dot coated with mercaptopropionic acid (2-MPA). *In vitro* studies reported in this work were conducted on a mouse fibroblast cell line (NIH/3T3) treated with Ag₂S/2-MPA quantum dots in 10-600 µg/mL concentration range for 24 h. Various fluorescence spectroscopy and microscopy methods were used to determine metabolic activity, proliferation rate and apoptotic fraction of QD-treated cells as well as QD internalization efficiency and intracellular localization. Metabolic activity and

proliferation rate of the QD treated cells were measured with XTT and CyQUANT[®] cell proliferation assays, respectively. Intracellular localization and qualitative uptake studies were conducted using confocal laser scanning microscopy. Apoptosis studies were performed with Annexin V assay. Finally, we also conducted a quantitative uptake assay to determine internalization efficiency of the silver sulfide particles.

Correlated metabolic activity and proliferation assay results indicate that Ag₂S/2-MPA quantum dots are highly cytocompatible with no significant toxicity up to 600 µg/mL treatment. Optimal cell imaging concentration was determined as 200 µg/mL. Particles displayed a punctuated cytoplasmic distribution indicating to endosomal entrapment.

In vitro characterization studies reported in this study indicate that Ag₂S/2-MPA quantum dots have great biological application potential due to their excellent spectral and cytocompatibility properties. Near-infrared emission of silver sulfide quantum dots provides a major advantage in imaging since signal interference from the cells (autofluorescence) which is a typical problem in microscopic studies is minimum in this part of the emission spectrum.

The results of this study are presented in an article which was accepted by Journal of Materials Chemistry. DOI: 10.1039/C2JM31959D.

Keywords: Quantum dot, cytocompatibility, localization, in vitro imaging

ÖZ

AG₂S/2-MPA KUANTUM NOKTACIKLARI; SİTO-UYUMLULUK VE HÜCRE İÇİ ALIM ÇALIŞMALARI

Erdem, Rengin

Yüksek Lisans, Biyoteknoloji Bölümü

Tez Yöneticisi: Yrd. Doç. Dr. Can Özen

Ortak Tez Yöneticisi: Doç. Dr. Havva Funda Yağcı Acar

Haziran 2012, 67 sayfa

Kuantum noktacıkları, yüksek kuantum verimi ve fotokararlılık gibi önemli optik özellikleri olan floresan yarı iletken nanokristallerdir. Bu nanopartiküller organik boyalara ve floresan proteinlere göre birçok açıdan üstündür ve bu nedenle hem in vivo hem de in vitro görüntüleme ve ilaç salımı uygulamalarında kullanılmak üzere büyük potansiyel göstermektedirler. Fakat sitotoksikite konusu hala kuantum noktacıklarının biyolojik uygulamaları ile ilgili önemli problemlerden birisidir.

Bu çalışmanın amacı, merkaptopropiyonik asit (2-MPA) ile kaplanmış bir özgün gümüş sülfid (Ag₂S) kuantum noktacığının in vitro karakterizasyonu ve biyolojik uygulamalar konusundaki potansiyelini değerlendirmektir. Bu çalışmada sunulan in vitro çalışmalar, 10 ile 600 µg/mL arasındaki konsantrasyonlarda, 24 saat süresince kuantum noktacığı uygulanmış fare fibroblast hücreleri (NIH/3T3) üzerinde yürütülmüştür. Çeşitli floresan spektroskopisi ve mikroskopisi metotları; KN uygulanmış hücrelerdeki metabolik aktivite, çoğalma hızı ve apoptoz oranı

değerlerinin belirlenmesi ile birlikte hücrelerin KN içselleştirilme etkinliği ve hücre içi lokalizasyon çalışmalarında kullanılmıştır. KN uygulanmış hücrelerin metabolik aktivitesi ve çoğalma hızı sırasıyla XTT ve CyQUANT® deneyleri ile ölçülmüştür. Hücre içi lokalizasyon ve nitel hücre içi alım çalışmaları konfokal lazer taramalı mikroskopisi ile yürütülmüştür. Apoptoz çalışmaları Annexin V deneyi ile yapılmıştır. Son olarak, gümüş sülfid partiküllerinin içselleştirme etkinliğinin belirlenmesi amacıyla nicel bir hücre içi alım deneyi uygulanmıştır.

Birbiriyle korrelasyon gösteren metabolik aktivite ve çoğalma hızı deneylerinin sonuçları Ag₂S/2-MPA kuantum noktacıklarının 600 µg/mL değerindeki konsantrasyonlara kadar oldukça sito-uyumlu olduğunu ve belirgin bir toksik etkiye sahip olmadığını belirtmektedir. Optimum hücre görüntüleme konsantrasyonu 200 µg/mL olarak belirlenmiştir. Parçacıklar noktalı sitoplazmik dağılım göstermiş olup; bu durum hem endozomlarda hapsedilmiş parçacıklar olduğunu göstermektedir.

Bu çalışmada sunulan in vitro karakterizasyon çalışmaları, Ag₂S/2-MPA kuantum noktacıklarının üstün spektral ve sitouyumluluk özellikleri sebebiyle biyolojik uygulamalar konusunda büyük potansiyele sahip olduğunu göstermektedir. Gümüş sülfid kuantum noktacıklarının kızılötesi civarındaki emisyonu ayrıca büyük bir avantaj sağlamaktadır çünkü hücrelerden gelen sinyal etkileşimi (otofloresan) bu emisyon spektrumunda çok zayıf kalmaktadır.

Bu çalışmanın sonuçları Journal of Materials Chemistry tarafından kabul edilmiş olan bir makalede sunulmuştur. DOI: 10.1039/C2JM31959D.

Anahtar Kelimeler: Kuantum noktacığı, hücre uyumluluğı, lokalizasyon, in vitro görüntüleme

To my family

ACKNOWLEDGEMENTS

First of all, special thanks go to my supervisor Assist. Prof. Dr. Can Özen. The supervision and support that he gave made the smooth progression of this thesis possible.

Another person that calls for special thanks is my co supervisor Assoc. Prof. Dr. Havva Funda Yağcı Acar for her guidance.

I would also like to express my gratitude towards Prof. Dr. Meral Yücel for her support.

Cell culture, microscopy and spectroscopy studies of this work have been completed at METU Central Laboratory Molecular Biology and Biotechnology R&D Center. Fluorescence spectroscopy support was provided by METU Center of Excellence in Biomaterials and Tissue Engineering (BIOMATEN) and Bilkent University National Research Center for Nanotechnology (UNAM).

I would like to state my appreciation to my lab mate Esen Sayın for her help. I would also like to thank Assist. Prof. Dr. Deniz Yücel for her help and advice about cell culture studies. I want to thank Assist. Prof. Dr. Sreeparna Banerjee, Assist. Prof. Dr. Elif Erson Bensan and Prof. Dr. Ufuk Gündüz for the materials and the precious knowledge they gracefully shared with us.

This study was supported by TUBITAK, Turkish Scientific and Technical Research Institute (109R031) and METU BAP, Scientific Research Project Coordination Office (BAP-07.02.2011.101).

Last but not least, I would like to thank my family for their support and love. Their encouraging presence was the reason of my perseverance. I would like to dedicate

this study to them.

TABLE OF CONTENTS

| | |
|--|-------|
| ABSTRACT..... | iv |
| ÖZ..... | vi |
| ACKNOWLEDGEMENTS..... | ix |
| TABLE OF CONTENTS..... | xi |
| LIST OF TABLES..... | xiv |
| LIST OF FIGURES..... | xv |
| ABBREVIATIONS..... | xviii |
| CHAPTERS | |
| 1. INTRODUCTION | 1 |
| 1.1 Quantum Dots (QDs)..... | 2 |
| 1.1.1 Structure of Quantum Dots..... | 2 |
| 1.1.2 Physical Properties of Quantum Dots..... | 3 |
| 1.1.3 Advantages..... | 5 |
| 1.1.4 Limitations..... | 8 |
| 1.1.5 Applications in Biology | 10 |
| 1.1.5.1 Cell Imaging..... | 10 |
| 1.1.5.2 In vivo Imaging..... | 12 |
| 1.1.5.3 Gene Technology..... | 13 |
| 1.1.5.4 Investigation of Toxins and Pathogens..... | 14 |
| 1.1.5.5 Quantum Dots as Biosensors..... | 15 |
| 1.1.5.6 Therapeutic Quantum Dots..... | 16 |
| 1.2 Ag ₂ S-(2-mercaptopropionic acid) Quantum Dots..... | 18 |
| 1.3 Cell Viability Assay..... | 20 |
| 1.4 CyQUANT® Cell Proliferation Assay | 22 |
| 1.5 Confocal Laser Scanning Microscopy..... | 23 |
| 1.6 Uptake Assay: Quantitative Determination of Internalization..... | 25 |
| 1.7 Apoptosis Analysis..... | 26 |
| 1.7.1 Working Principle..... | 26 |

| | | |
|---------|---|----|
| 1.7.2 | Microfluidic Cell Chips..... | 27 |
| 1.8 | Aim of the Study..... | 28 |
| 2. | EXPERIMENTAL | 30 |
| 2.1 | Materials | 30 |
| 2.1.1 | Cell Lines | 30 |
| 2.1.2 | Chemicals & Reagents..... | 30 |
| 2.1.3 | Ag ₂ S-(2-mercaptopropionic acid) Quantum Dots..... | 31 |
| 2.2 | Methods | 31 |
| 2.2.1 | Cell Culture | 31 |
| 2.2.1.1 | Cell Culture Conditions..... | 31 |
| 2.2.1.2 | Subculturing..... | 31 |
| 2.2.1.3 | Cell Stock Preparation..... | 31 |
| 2.2.1.4 | Stock Thawing..... | 32 |
| 2.2.1.5 | Viable Cell Count with Trypan Blue..... | 32 |
| 2.2.2 | Spectral Analysis of Quantum Dots..... | 32 |
| 2.2.3 | XTT Assay..... | 33 |
| 2.2.4 | Proliferation Assay..... | 33 |
| 2.2.5 | Fixed Cell Imaging..... | 34 |
| 2.2.6 | Uptake Assay..... | 35 |
| 2.2.7 | Annexin V Based Apoptosis Assay..... | 36 |
| 2.2.7.1 | Sample Preparation..... | 36 |
| 2.2.7.2 | Chip Loading and Running..... | 37 |
| 2.2.7.3 | Data Analysis..... | 37 |
| 2.2.8 | Statistical Analysis..... | 38 |
| 3. | RESULTS AND DISCUSSION..... | 39 |
| 3.1 | Cytocompatibility | 39 |
| 3.1.1 | Metabolic Activity Determination with XTT Assay..... | 39 |
| 3.1.1.1 | Assay Optimization..... | 39 |
| 3.1.1.2 | Variation in the Metabolic Activity..... | 41 |
| 3.1.2 | Nucleic Acid Content Determination with Proliferation Assay.... | 42 |
| 3.1.2.1 | Standard Curve for Cell Number..... | 43 |
| 3.1.2.2 | Variation in Cell Proliferation..... | 43 |

| | |
|---|----|
| 3.2 Cellular Internalization and Localization..... | 44 |
| 3.2.1 Cell Imaging..... | 44 |
| 3.2.2 Quantification of Uptake..... | 46 |
| 3.2.2.1 Optimization Studies..... | 46 |
| 3.2.2.2 Calibration Curve Preparation..... | 48 |
| 3.2.2.3 Uptake of Ag ₂ S Quantum Dots..... | 49 |
| 3.3 Cytotoxicity: Necrosis vs. Apoptosis..... | 49 |
| 4. CONCLUSION..... | 54 |
| REFERENCES..... | 56 |
| APPENDICES | |
| A. MEDIUM SPECIFICATIONS..... | 64 |
| B. SOLUTIONS..... | 66 |

LIST OF TABLES

TABLES

| | |
|--|----|
| Table 2.1 Excitation scan wavelength settings | 33 |
| Table 3.1 Percentage of apoptotic, healthy and necrotic cells in untreated, etoposide and QD treated NIH/3T3 cells..... | 53 |
| Table A.1 MEM liquid medium with Earle's salts, NaHCO ₃ and stable glutamine | 64 |
| Table A.2 DMEM liquid medium with stable glutamine, 3.7 g/L NaHCO ₃ , 1.0 g/L D-glucose..... | 65 |

LIST OF FIGURES

FIGURES

| | |
|---|----|
| Fig 1.1 A: Transmission electron micrograph of QDs, B: Schematic diagram of QD layers..... | 2 |
| Fig 1.2 Comparison of QD's dimensional properties with other biological structures..... | 3 |
| Fig 1.3 Schematic diagram of the relation between size and band gap..... | 4 |
| Fig 1.4 Fluorescence emitting CdSe core, ZnS shell QDs whose emission wavelengths are changeable with core size increments from 2 nm to 7 nm (near UV excitation)..... | 4 |
| Fig 1.5 The electromagnetic spectrum..... | 5 |
| Fig 1.6 Excitation and emission spectrum expressed in arbitrary units (au) of CdSe QD and rhodamine 6G (an organic fluorophore) | 6 |
| Fig 1.7 Graph demonstrating the shift towards IR region of emission spectrum by the increase of size..... | 6 |
| Fig 1.8 Absorption and emission spectra of Alexa Fluor 594 dye and Qdot 625..... | 7 |
| Fig 1.9 Emission spectra of QD 510 and rhodamine..... | 7 |
| Fig 1.10 Molecular structure of TOPO..... | 8 |
| Fig 1.11 Schematic display of some metabolic pathways that are activated by the cytotoxic effects of CdTe QDs..... | 9 |
| Fig 1.12 QD application methods..... | 10 |
| Fig 1.13 Cellular structures stained with QDs: Nucleus, Golgi apparatus, tubulin..... | 11 |
| Fig 1.14 X and Y coordinate image of a vesicle containing QDs..... | 11 |
| Fig 1.15 Prostate cancer site labeled with red/orange fluorescence emitting QD..... | 12 |
| Fig 1.16 Images of a chicken embryo treated with Qtracker® (emission: 705 | |

| | |
|--|----|
| nm)..... | 13 |
| Fig 1.17 Micrograph of <i>C. parvum</i> and <i>G. lamblia</i> after immunofluorescent staining..... | 14 |
| Fig 1.18 Some utilizations of QDs as biosensors..... | 16 |
| Fig 1.19 Diagram showing some QD labeling methods..... | 17 |
| Fig 1.20 Summary of biological applications of the QDs..... | 18 |
| Fig 1.21 Chemical structure of the 2-MPA..... | 19 |
| Fig 1.22 Aqueous synthesis of 2-MPA coated Ag ₂ S..... | 19 |
| Fig 1.23 Excitation and emission spectra of Ag ₂ S/2-MPA QDs..... | 20 |
| Fig 1.24 UV spectra of the XTT (dotted) and formazan..... | 21 |
| Fig 1.25 The differences of experiment procedures between MTT and XTT..... | 21 |
| Fig 1.26 Cleavage of XTT which produces formazan..... | 22 |
| Fig 1.27 Spectrum of DNA bound CyQUANT GR dye..... | 23 |
| Fig 1.28 Diagram showing optical pathway and basic apparatus of CLSM..... | 24 |
| Fig 1.29 Comparison of widefield microscopy to confocal laser scanning microscopy images..... | 24 |
| Fig 1.30 Optical sections of lodgepole pine (<i>Pinus contorta</i>) pollen grain..... | 25 |
| Fig 1.31 Ex and em spectra of the calcein AM and cy5..... | 26 |
| Fig 1.32 A representative image for the annexin V conjugated Cy5 and calcein based staining for apoptosis detection..... | 27 |
| Fig 1.33 Solutions and their placements on the chip..... | 28 |
| Fig 1.34 Diagram of the microfluidic system..... | 28 |
| Fig 2.1 Diagram for apoptosis staining..... | 37 |
| Fig 3.1 Optimization of XTT reaction solution volume..... | 40 |
| Fig 3.2 Optimization of XTT reagent incubation time for NIH/3T3 cells..... | 40 |
| Fig 3.3 The absorbance difference between medium with and without phenol red..... | 41 |
| Fig 3.4 XTT results of QD treatments with various concentrations in NIH/3T3 cells after 24 hours of incubation..... | 42 |
| Fig 3.5 Standard curve for the proliferation assay of NIH/3T3 cells..... | 43 |
| Fig 3.6 Proliferation assay results of QD treatments with various concentrations in NIH/3T3 cells after 24 hours of incubation..... | 44 |

| | |
|--|----|
| Fig 3.7 CLSM images of NIH/3T3 cells treated with 200 ug/mL QD for 24 hrs..... | 45 |
| Fig 3.8 Fluorescence scan of 0.16 nM Qdot 565 ITK Carboxyl in complete medium and in PBS..... | 47 |
| Fig 3.9 Emission scans of untreated and treated (with 16 nM Qdot 565 ITK Carboxyl) samples which were seeded with 50,000 cells..... | 47 |
| Fig 3.10 Emission scans of untreated, treated with 16 nM Qdot 565 ITK Carboxyl and treated with 32 nM Qdot 565 ITK Carboxyl samples which were seeded with 250,000 cells..... | 48 |
| Fig 3.11 Calibration curve for uptake assay of Qdot 565 ITK Carboxyl..... | 48 |
| Fig. 3.12 Dot plot of events in terms of fluorescence intensity | 51 |
| Fig. 3.13 Histogram of events in terms of fluorescence intensity | 52 |

ABBREVIATIONS

| | |
|-------------------------|---|
| QD | Quantum dot |
| DMSA | Meso-2-3-dimercaptosuccinic acid |
| 2-MPA | 2-mercaptopropionic acid |
| 3-MPA | 3-mercaptopropionic acid |
| PEG | Polyethylene glycol |
| Ag₂S | Silver sulfide |
| CdTe | Cadmium telluride |
| CdS | Cadmium sulfide |
| CdSe | Cadmium selenide |
| ZnS | Zinc sulfide |
| ZnSe | Zinc selenide |
| InAs | Indium arsenide |
| InP | Indium phosphide |
| Na₂Te | Sodium Telluride |
| CLSM | Confocal Laser Scanning Microscopy |
| XTT | Sodium 3'-[1-(phenylaminocarbonyl)- 3,4-tetrazolium]-bis (4-methoxy-6-nitro) benzene sulfonic acid hydrate |
| ELISA | Enzyme Linked Immunosorbent Assay |
| FBS | Fetal Bovine Serum |
| PBS | Phosphate Buffered Saline |
| MEM | Minimum Essential Medium |
| DMEM | Dulbecco's Modified Eagle's Medium |
| EDTA | Ethylenediaminetetraacetic acid |
| Cd | Cadmium |
| RFU | Relative Fluorescence Units |
| UV | Ultraviolet |
| ex | Excitation |
| em | Emission |
| FDA | Food and Drug Administration |

| | |
|------------|-------------------------|
| ROS | Reactive Oxygen Species |
| NIR | Near Infrared Region |

CHAPTER 1

INTRODUCTION

Nanotechnology is the science of developing unique structures and machines from individual atoms and molecules. In 1970's, first quantum wells were consisted of semiconductors which had its electrons restricted in two dimensions. Then came quantum wires with electrons confined in one dimension and quantum dots with electrons confined in zero dimension (Reed et al, 1993).

Due to their significantly advantageous properties, quantum dots can replace the material that is used to manufacture many industrial products. For instance, pen inks containing QDs can be a solution for fraud and light emitting diodes (LEDs) produced with QDs would illuminate more efficiently. Thermoelectric devices that can produce electricity from thermal energy can be made of QDs. Furthermore, QDs can replace current semiconductor solar cells because they would use sun energy more efficiently (Nanoco Technologies, 2011).

Nanobiotechnology, a branch of the nanotechnology, investigates the biological systems in order to improve tools inspired from the biology itself (Mongillo et al, 2007). Gold nanoparticles, iron nanoparticles, biological nanoparticles and quantum dots (QDs) are some of the devices that are appropriate for biological applications. Biological nanoparticles such as viruses can be used for nanosensor and nanobead manufacturing and gold nanoparticles can be conjugated with DNA for the biodiagnostic systems. Since these nanoparticles are very small, the internalization is highly efficient. Also, enhanced area to volume ratio helps the diffusion and they are not easily degraded by heat and chemicals. These nano devices are expected to be the precursors of future modellings for a toolbox which will be used in biology and nanomedicine (Kumar et al, 2011).

1.1 Quantum Dots (QDs)

1.1.1 Structure of Quantum Dots

Quantum dots are semiconductor nanocrystals that have unique spectral properties. Their diameter size ranges between 2 to 6 nm and can carry 10 to 50 atoms (Nanoprint Technologies, 2008). The innermost part of a QD is the core which is the section that gives the QD its high fluorescence emission ability. The core can be composed of II and VI group elements (e.g. CdTe, CdSe, ZnSe and CdS) or II and VI group elements (e.g. InAs and InP) (Chan et al, 2002). After the core comes the shell which is made of semiconductors (ZnS, etc.). Shell layer adds stability to the core structure. A separate polymer (PEG, etc) layer can be added onto the shell layer in order to produce more biocompatible and water soluble QDs (Invitrogen, 2006). Finally, for targeting purposes, biomolecules such as oligonucleotides, antibodies and peptides can be used to build QD bioconjugates (Fig 1.1) (Vashist et al, 2006).

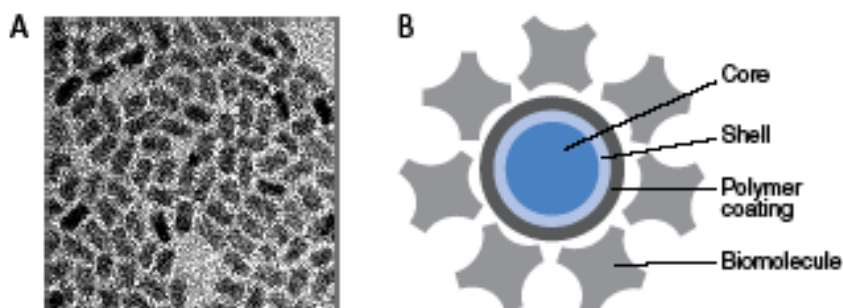


Fig 1.1 A: Transmission electron micrograph of QDs, B: Schematic diagram of QD layers (Invitrogen, 2006).

QDs can be shaped into spheres, rods or tetrapods, however for biological applications, spherical QDs are preferred (Smith et al, 2004).

Various layers that can be further attached onto QDs make the final QD size close to the size of a protein molecule (Invitrogen, 2006) (Fig 1.2).

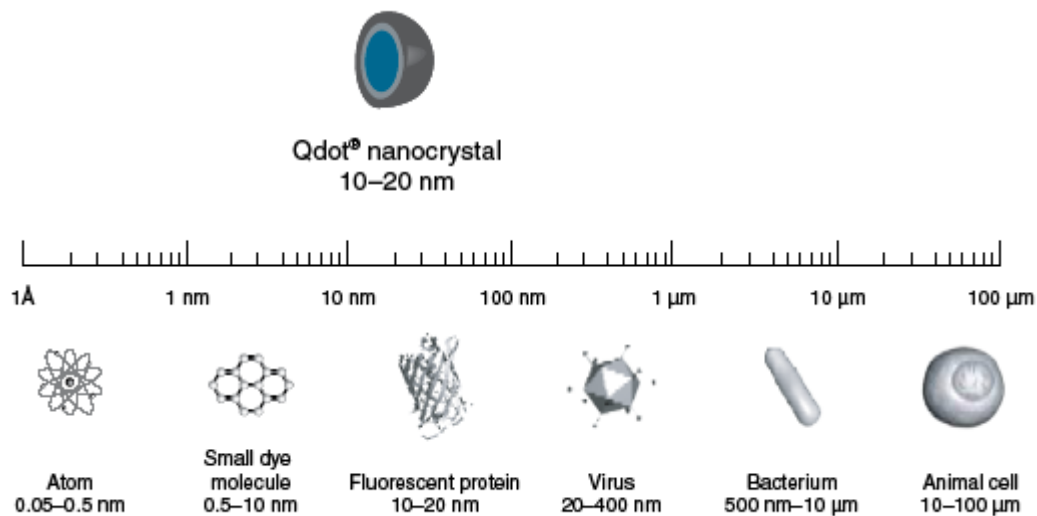


Fig 1.2 Comparison of QD’s dimensional properties with other biological structures (Invitrogen, 2006).

1.1.2 Physical Properties of Quantum Dots

When a photon excites the electron at the valence band, a semiconductor emits fluorescence. Excited electron, creating a positively charged hole, departs from the valence band relocates on the conductance band. Translocated electron and the hole that is the result of the excitation of the electron forms an exciton. The exciton Bohr radius is larger than the physical size of the QD. However, the bulk semiconductor is larger than the exciton Bohr radius. This creates the quantum confinement effect. A QD requires more energy than a bulk semiconductor for the production of an exciton. Furthermore, in a bulk semiconductor energy levels remain continuous whereas the energy levels of a QD are discrete (Fig 1.3). The emission spectrum is dependent on the physical size of the QD since the bandgap energy is variable with the size of the core (Fig 1.3) (Nagy et al, 2010). In addition to this trait, the material used for the production of the QD can also change the spectral characteristics of the QD (Fig 1.4) (Han et al, 2001).

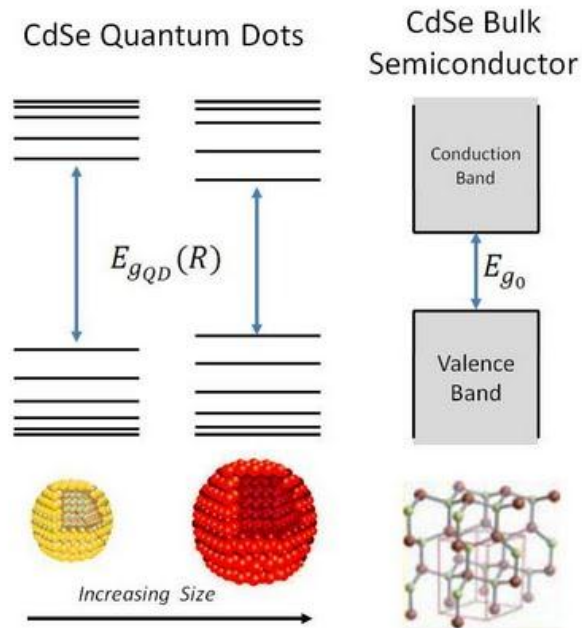


Fig 1.3 Schematic diagram of the relation between size and bandgap (Hughes et al, 2008).



Fig 1.4 Fluorescence emitting CdSe core, ZnS shell QDs whose emission wavelengths are changeable with core size increments from 2 nm to 7 nm (near UV excitation) (Han et al, 2001).

The emission spectrum of the QD can be shifted along the 400 nm and 2000 nm. Therefore emission can be achieved at near UV, visible and near infrared ranges (Fig 1.5) (Smith et al, 2004).

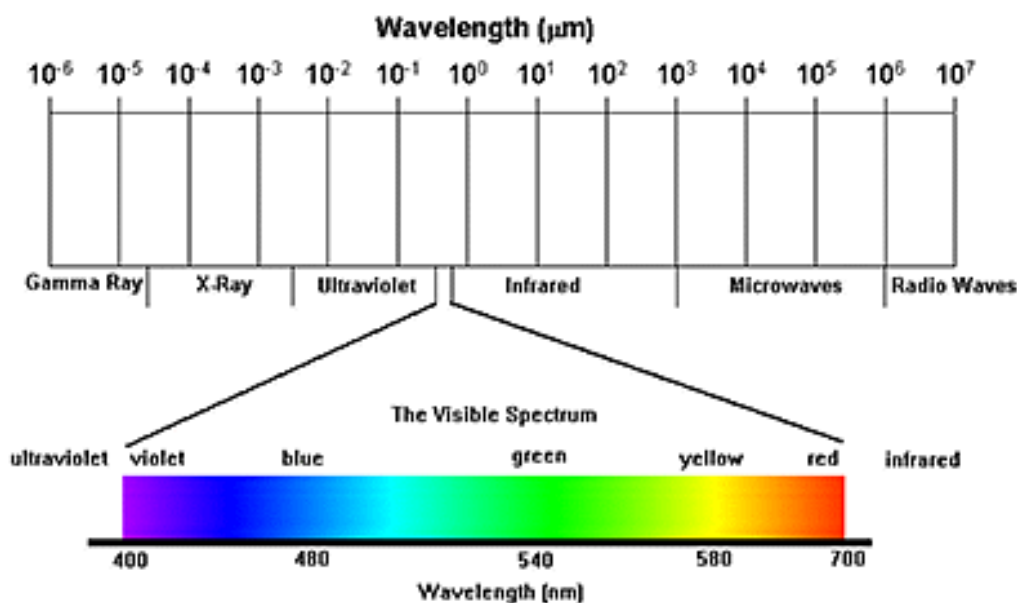


Fig 1.5 The electromagnetic spectrum (CRISP, 2001).

1.1.3 Advantages

Quantum dots possess several advantageous qualities over organic dyes such as fluorescein and fluorescent probes like green fluorescent protein (GFP). Contemporarily, organic dyes are incorporated in various targeting and imaging methods, however, these methods can be further improved with the replacement of QDs with organic dyes (Smith et al, 2004). QDs provide a wide range of choices for the excitation wavelength since they have a broad excitation spectra. On the other hand, organic dyes have narrow wavelength spectra which limits the user (Jaimeson et al, 2007).

Organic dyes have large emission spectra which cause channel cross-talk when multiple organic dyes are applied to the same sample because of spectral overlap (Jaiswal et al, 2004). In contrast to this, QDs have narrow emission spectra that minimizes the risk of overlap between different QDs (Fig 1.6). Another superior feature of QDs is that their emission spectra is also size-tunable. Modifications on physical dimensions and core and coating material can create different emission behavior ranging from UV to IR wavelengths (Fig 1.7) (Jaimeson et al, 2007).

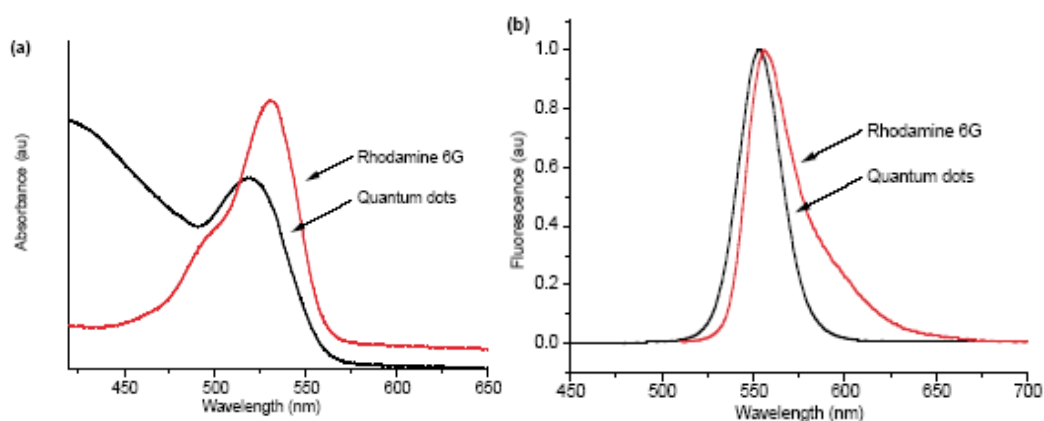


Fig 1.6 Excitation (a) and emission (b) spectrum expressed in arbitrary units (au) of CdSe QD (black line) and rhodamine 6G (an organic fluorophore) (red line). (Jaimeson et al, 2007).

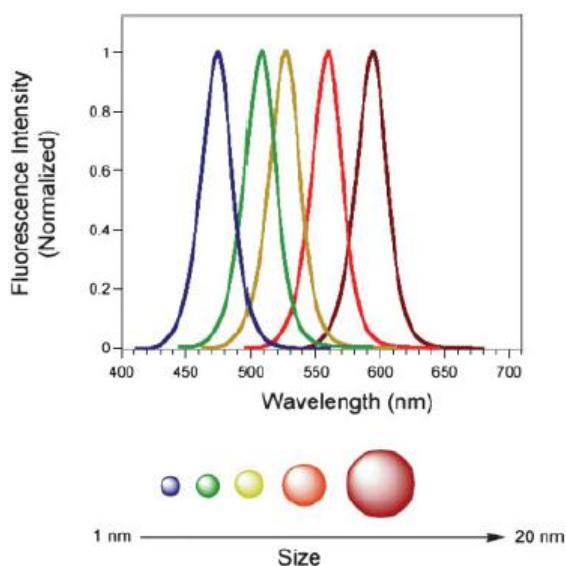


Fig 1.7 Graph demonstrating the shift towards IR region of emission spectrum by the increase of size (Zhou et al, 2007).

Another advantage of QDs over organic dyes is their higher photostability which means that they emit fluorescence for a far longer time than organic dyes when they are excited. Thus, QDs are very compatible for long term imaging and targeting applications (Smith et al, 2004).

QD molar extinction coefficient is higher than that of organic dyes as well (Fig 1.8)

(Invitrogen, 2011). Higher molar extinction coefficient provides much more light absorption from the excitation source. Therefore, a QD can be excited more efficiently with a weak light source than an organic fluorophore.

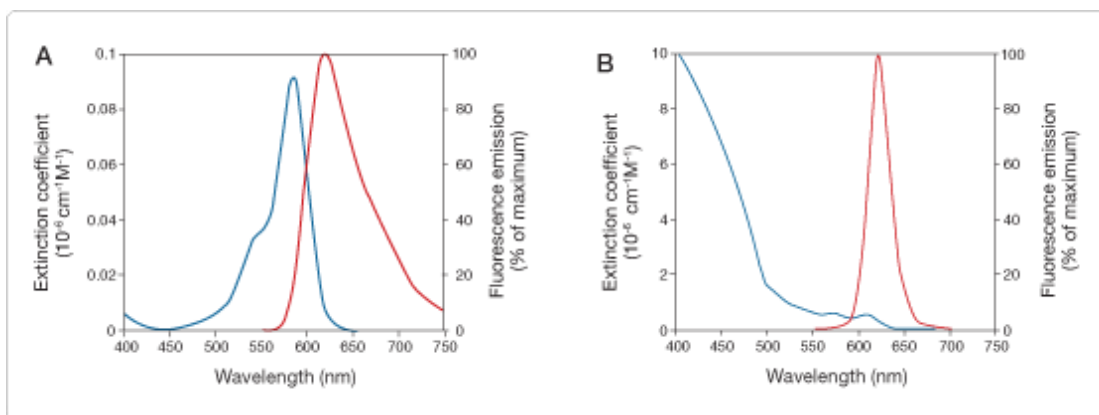


Fig 1.8 Absorption (blue) and emission (red) spectra of Alexa Fluor 594 dye (a) and Qdot 625 (b) (Invitrogen, 2011).

QDs have high Stoke's shifts which can be described as the distance between the excitation and the emission spectra. With high Stoke's shift, the excitation signal does not interfere with the emission signal (Fig 1.9) (Jaiswal et al, 2004).

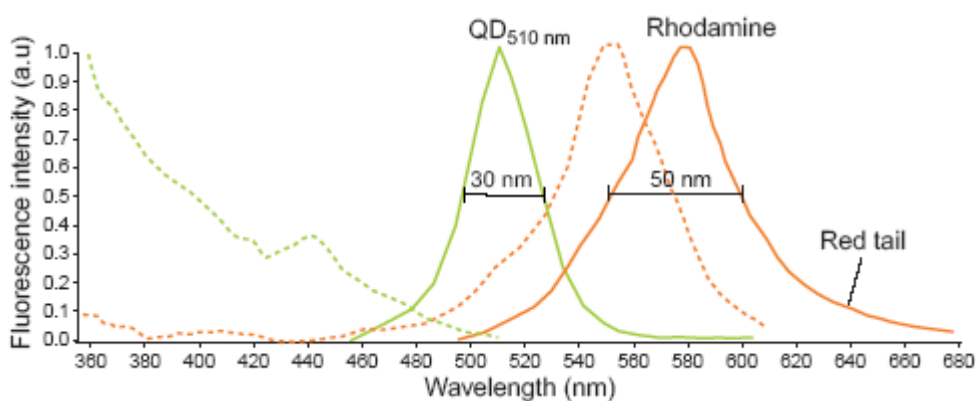


Fig 1.9 Emission spectra of QD 510 and rhodamine (Jaiswal et al, 2004).

Large quantum yield is another quality that makes QDs more superior over organic fluorophores. A larger quantum yield means the higher likelihood of the fluorescence emission rather than the nonradiative energy release during the relaxation of the excited molecule (Jaiswal et al, 2004).

1.1.4 Limitations

The basic approach for the synthesis of QDs is utilization of organic solvents such as chloroform or toluene at high temperatures. This method results in an outer layer of a surfactant like TOPO (trioctylphosphine oxide) (Fig 1.10) on the QD. This surfactant layer renders QD insoluble in aqueous environment since the hydrophilic side of it is attached to the core and the apolar side stretches outwards.

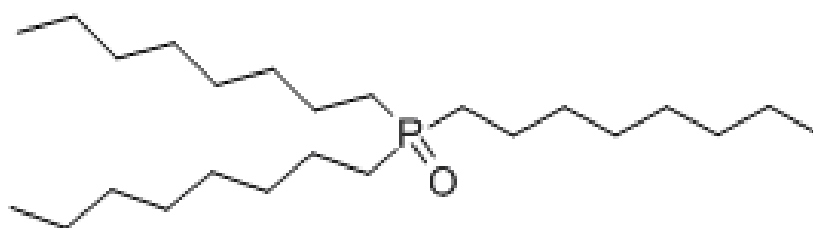


Fig 1.10 Molecular structure of TOPO (Chemical Book, 2010).

However, biological applications need water soluble QDs due to the hydrophilic nature of the cells and living tissues. In order to create water soluble QDs, ligands with outer polar groups which are bound to the QD with functional elements can be used to replace the surfactant layer. Another method is to cover the hydrophobic surface of the QD with polar and amphipathic polymers. Finally, phospholipid micelles can be used to envelop the QD (Vashist et al, 2006).

Targeted localization inside the cell can be difficult with quantum dots. QDs are internalized by cells through endocytosis that delivers them first to early endosomes and then to late endosomes and lysosomes. Hydrolyzes that reside in these secondary destinations is claimed to cause QD aggregates because of the low pH conditions they induce (Zhang et al, 2009). Therefore, QDs are trapped and degraded before they can reach their destination (El-Sayed et al, 2009). Also, even the endocytosis itself can be problematic since QDs are considerably large particles. In addition to this drawback, large size can also clog up the cytoplasm and cause metabolic disruptions (Biju et al, 2008).

QDs are found to cause a decrease of metabolic activity in the cell (Lovric et al, 2005). The magnitude of this effect is dependent on size, core and capping materials, treatment concentration and surface activity. Another cytotoxic outcome is free heavy metals that create free radicals (Lovric et al, 2005). If the capping material is not stable enough, heavy metal (Cd^{+2}) can be released from the QD core. The release of heavy metals can also be induced by excitation of the QD by a UV light source (Fig 1.11) (Jaimeson et al, 2007). The UV light itself causes free radicals as well.

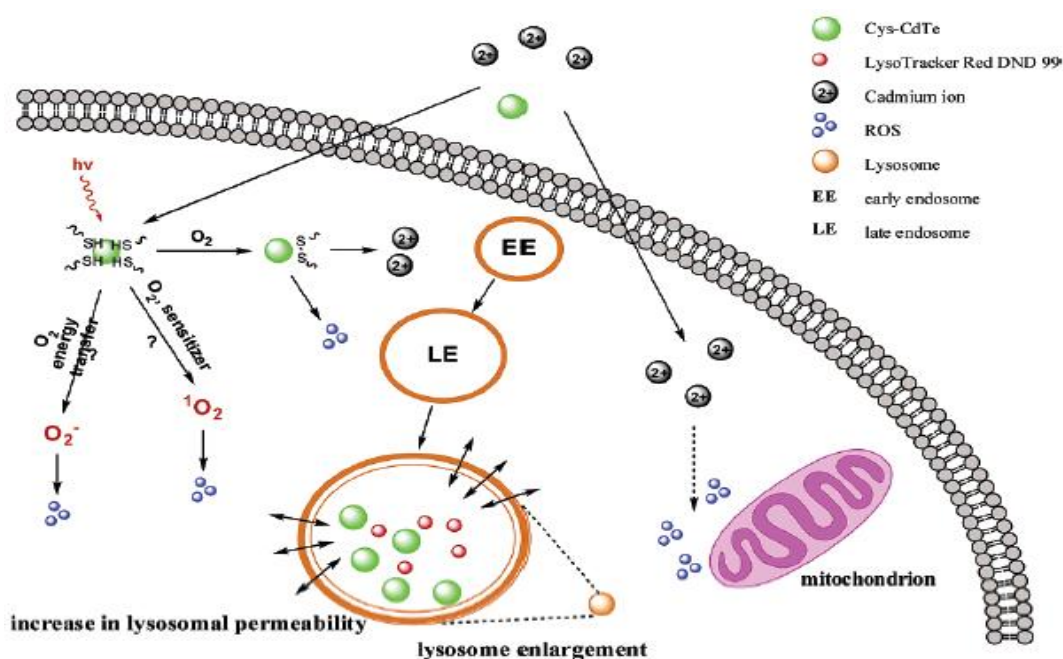


Fig 1.11 Schematic display of some metabolic pathways that are activated by the cytotoxic effects of CdTe QDs (Cho et al, 2007).

Reactive oxygen species production triggers apoptosis. Cytochrome c is released to the cytosol during the apoptosis. Apoptosis was detected after CdTe QD treatment to MCF-7 cells by measuring the cytochrome c levels in the cytosol which is a molecule that is released from the intermembrane space of the mitochondria during apoptosis (Lovric et al, 2005).

1.1.5 Applications in Biology

1.1.5.1 Cell Imaging

Quantum dots can be delivered into the cells by employing various techniques (Fig 1.12) (Biju et al, 2008). They can also be targeted into a certain organelle or a cellular structure such as Golgi, mitochondria, nucleus etc. Invitrogen QDot nanoparticles were conjugated to antibodies or streptavidin and were used to stain HeLa cells (Fig 1.13) (Invitrogen, 2006).

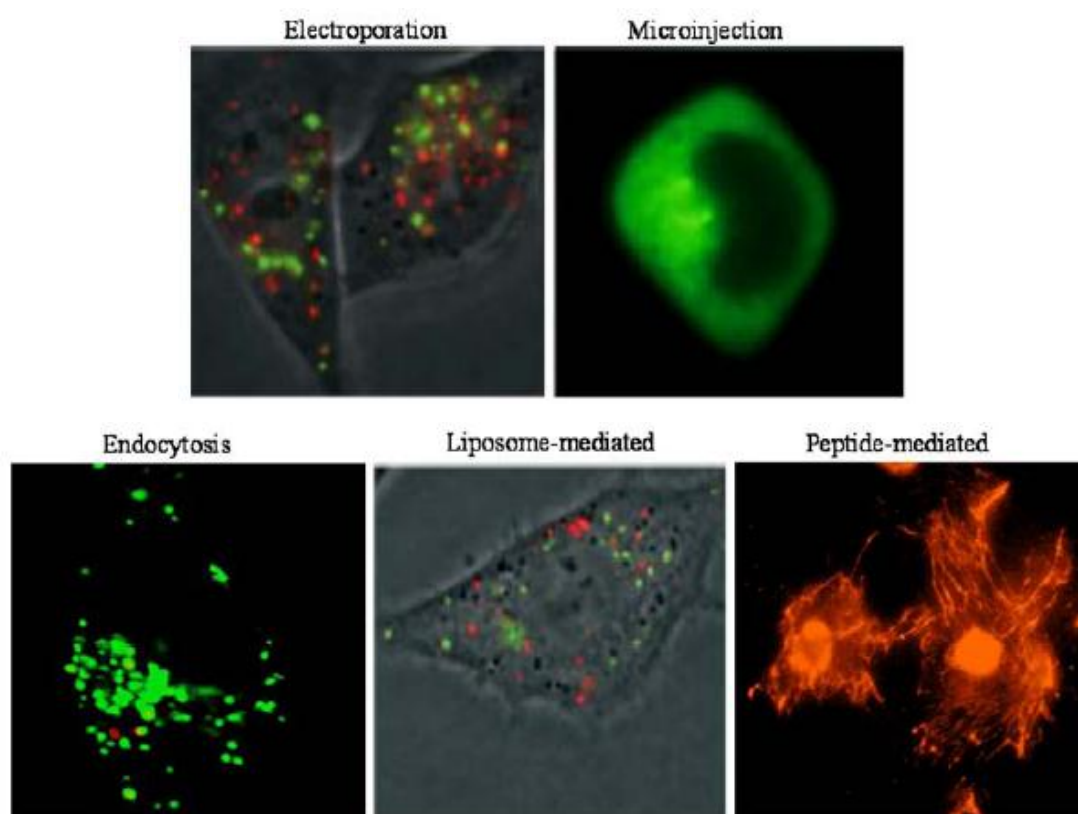


Fig 1.12 QD application methods (Biju et al, 2008).

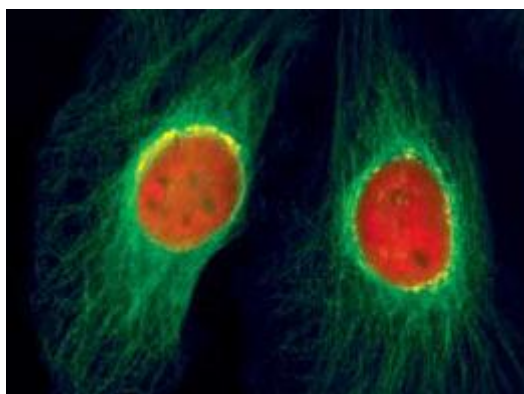


Fig 1.13 Cellular structures stained with QDs: Nucleus (red), golgi apparatus (yellow), tubulin (green) (Invitrogen, 2006).

A cell membrane receptor called Her2 is overexpressed in cancerous cells. Since this is an unique case, Her2 can be used as a breast cancer marker and can be detected with secondary antibody conjugated QDs (Biju et al, 2008).

QDs can also be utilized for real time live cell imaging. For example, cargo transfer from cell membrane to perinuclear area was observed and it was found that the translocation takes place at dynein direction with a 1.5 $\mu\text{m/s}$ velocity in A549 (human lung cancer) cells (Nan et al, 2005).

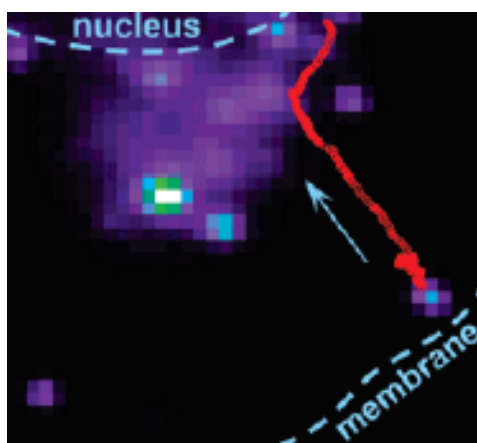


Fig 1.14 X and Y coordinate image of a vesicle containing QDs (Nan et al, 2005).

1.1.5.2 In Vivo Imaging

CdSe core ZnS shell QDs were used to target blood vessels, tumors and lymph node. These QDs had near infrared (NIR) emission which offers noninvasive deep tissue imaging. By the use of this technique, surgeons can detect lymph nodes that reside around a cancerous organ and may contain metastatic cells prior to or during operation (Biju et al, 2008).

In another study, a QD with PEG coating and prostate membrane targeted antigen conjugate was utilized for in-vivo observation of prostate tumor in nude mice (Fig 1.15). Only PEG coated QDs were mainly located at the tumor site due to the increased permeability of the cancer tissue. However, tumor collection efficiency was higher for the antigen conjugated QDs (Gao et al, 2004).

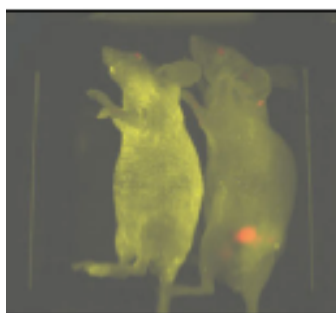


Fig 1.15 Prostate cancer site labeled with red/orange fluorescence emitting QD. Mouse on the left is healthy (Gao et al, 2004).

Blood vessels were observed using PEG coated Qtracker® commercial QD from Invitrogen. Red emission with extended lifetime provides the deep tissue imaging with no extra injection at small sized animals (Fig 1.16) (Invitrogen, 2006).

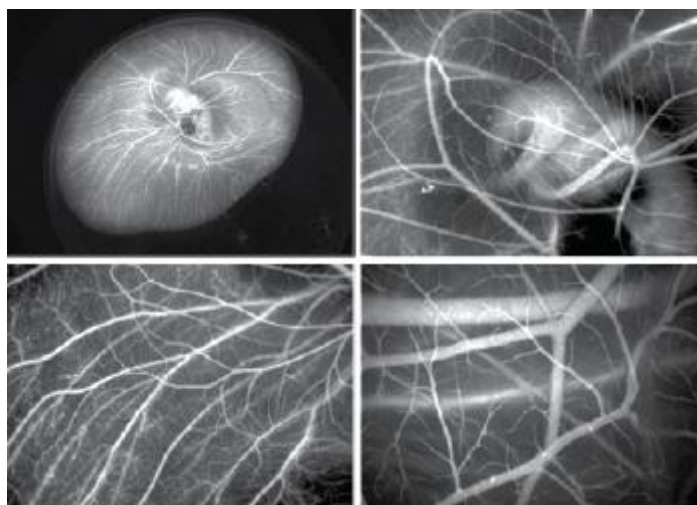


Fig 1.16 Images of a chicken embryo treated with Qtracker® (emission: 705 nm) (Invitrogen, 2006).

Lymphocyte immunology and developmental biology are couple of examples to other research areas that can benefit from in vivo imaging with QDs where tracking the movements of even one cell is possible (Banerjee et al, 2010).

1.1.5.3 Gene Technology

Quantum dots attached to oligonucleotides through carboxylic acid groups were used to label DNA or mRNA in fluorescence in situ hybridization (FISH) method. This approach was employed as a breast cancer detector by labeling ERBB2/HER2/neu locus which is associated mainly with breast tumors. It was concluded that when the experiments were conducted with QDs, fluorescence intensity and stability was much better than when organic dyes were applied (Jaimeson et al, 2007).

Different colored QDs microbeads have been used to detect single nucleotide polymorphisms (SNPs) with flow cytometer. Also dynamic events at nucleotide levels like DNA replication and telomere lengthening have been observed using fluorescence resonance energy transfer (FRET) application in which QDs were incorporated (Jaimeson et al, 2007).

Luteotropic hormone and growth hormone siRNAs located in the brain were observed by in situ hybridization with QDs. iRNA bound QDs can be used to measure gene silencing in terms of fluorescence intensity (Jaimeson et al, 2007).

1.1.5.4 Investigation of Toxins and Pathogens

Pathogens such as *E. coli* 0157:H7, *G. lamblia*, *S. typhi*, *L. monocytogenes* and *C. parvum* have been observed by QD staining. Furthermore, it was made possible to detect both *G. lamblia* and *C. parvum* in one sample when two QDs with different emission spectra were used (Fig 1.17). QDs' superior fluorescence properties make them more preferable than other assays (Jaimeson et al, 2007).

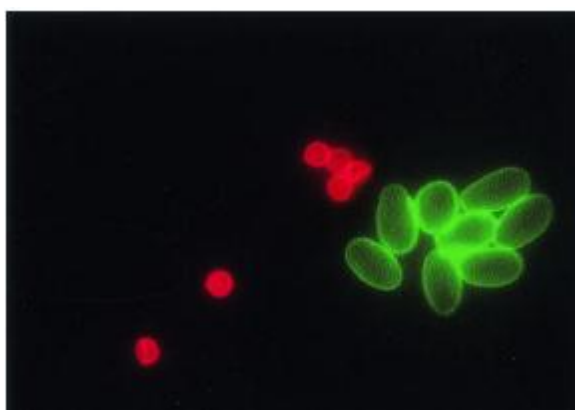


Fig 1.17 Micrograph of *C. parvum* (red) and *G. lamblia* (green) after immunofluorescent staining (Jaimeson et al, 2007).

Cholera toxin (CT), ricin, and Shiga-like toxin 1 (SLT-1) were all detected in one sample. It was possible to detect Staphylococcal enterotoxin B even in one digit ng/mL levels. Some problems concerning antibody specificity and cross-reactivity have been encountered but it is claimed that further studies would be able to overcome these obstacles (Jaimeson et al, 2007).

1.1.5.5 Quantum Dots as Biosensors

QDs can be highly convenient FRET donors since their emission wavelength range can be fine-tuned and is very narrow which is a quality that reduces the risk of inadvertent acceptor excitation. Acceptor can be another QD or another nanoparticle, even an organic dye (Bailey et al, 2004).

Quantum dots with different colors and intensities can be incorporated into polymer microbeads with various combinations. Variety coming from many color and intensity combinations can create 10^6 different color codes that can be read by a spectrofluorometer. Organic dyes, which are not as versatile as QDs, can produce only 100 codes. This technology can be used to develop new bioanalytical detection assays (Bailey et al, 2004).

As an alternative use of biosensor QDs maltose determination can be achieved with the maltose binding protein conjugation on QDs. Sugar-quencher molecules are attached additionally to the QDs. When these QDs are excited, the emission does not take place because the quencher absorbs the energy nonradiatively. If maltose is present in the solution, sugar-quencher molecule dissociates and maltose binds to the maltose binding protein. As a result of the dissociation of the sugar-quencher molecule, QD emits green wavelength. Second, single stranded DNA (ssDNA) can be determined using complementary DNA sequences conjugated with a dye and biotin separately. When streptavidin conjugated QD added to the sample and excited, energy is transferred to the dye molecule emits red fluorescence. Therefore, by the help of these systems amount of the maltose and ssDNA in the environment can be calculated by using the measured signal intensity. Third, bioluminescence resonance energy transfer (BRET) is another application for biosensor QDs. Quantum dot attached to a luciferase enzyme can emit fluorescence when luciferin is added to the environment because of the enzymatic reaction between the luciferase and luciferin. Luciferase speeds up the oxidation of the luciferin and as the result of this reaction bioluminescence appears (Fig 1.18) (Smith et al, 2008).

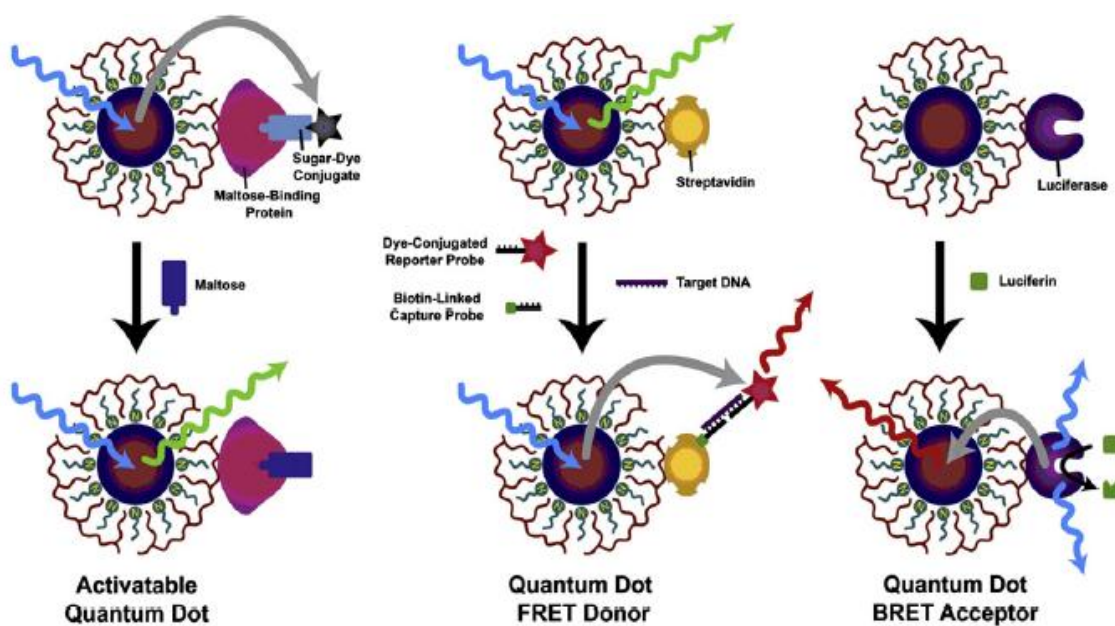


Fig 1.18 Some utilizations of QDs as biosensors (Smith et al, 2008).

1.1.5.6 Therapeutic Quantum Dots

Various approaches can be utilized for therapeutic uses of the QDs. Laser excitation of the QD can heat the solution and give rise to the formation of the bubbles. Mechanic act of the bubble effect and heat can destroy the tumor. Additionally, if the laser application annihilates the biocompatible layer of the QD, the core of the QD will be exposed and toxicity of the heavy metal will have a plus detrimental effect on the tumor (Berger et al, 2008).

Latest studies show the importance of the size of the drug carrier, as the production of the nanocrystals develops. QDs can be advantageous carriers because of the large surface area to volume ratio of the QD. Therefore, features like several attachment sites and small size of the carrier are possible with the QDs. While hydrophobic drugs can be embedded between the QD core and amphiphilic polymer coating, hydrophilic drugs (small interfering RNA (siRNA), antisense oligodeoxynucleotide, peptide, aptamer and antibody) can be attached to the external side of the QD. Real time imaging, cell specific recognition and treatment are the advantages of this QD composition (Fig 1.19) (Qi et al, 2008).

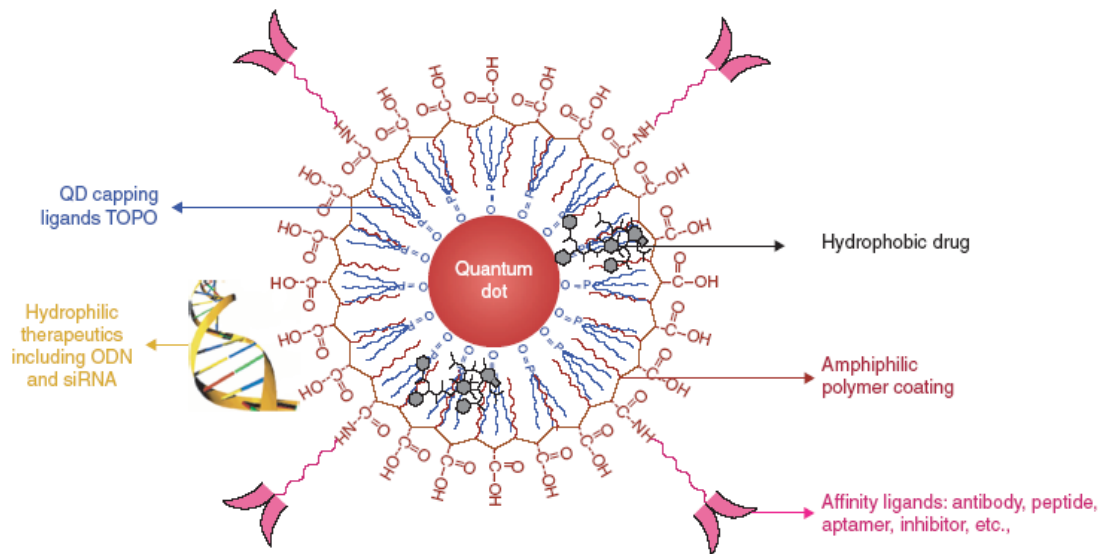


Fig 1.19 Diagram showing some QD labeling methods (Qi et al, 2008)

Main applications of the QDs can be summarized as Fig 1.20.

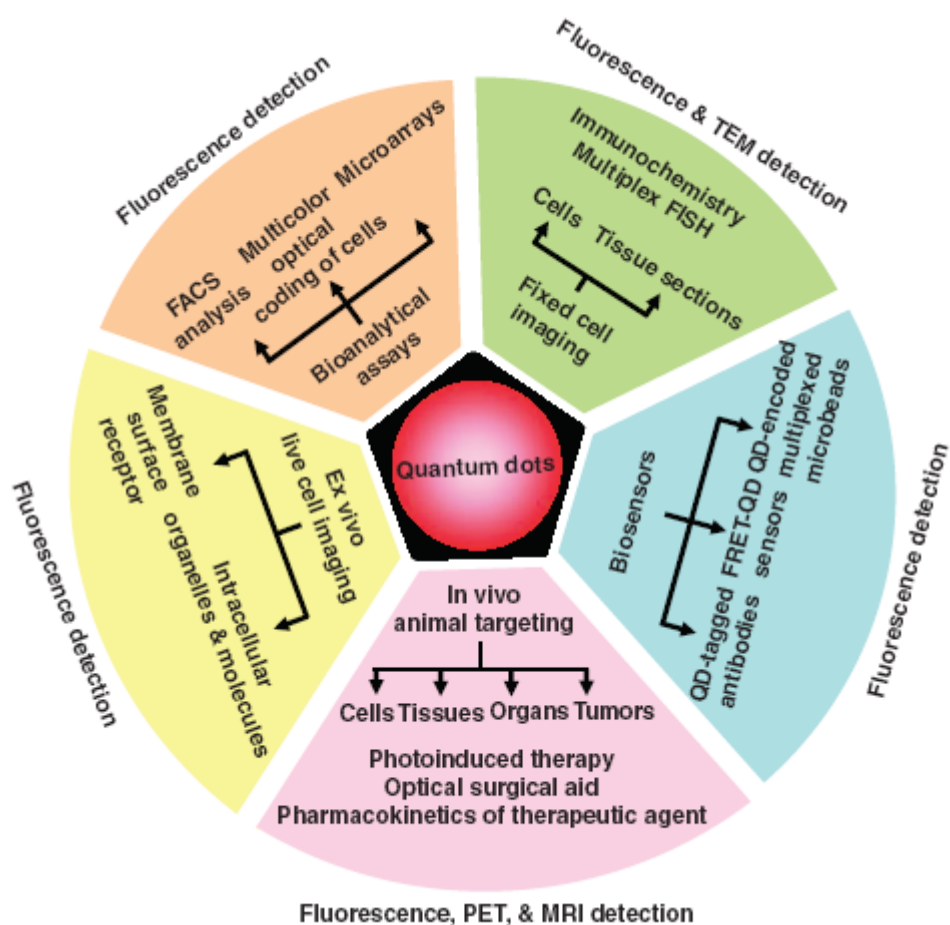


Fig 1.20 Summary of biological applications of the QDs (Michalet et al, 2005).

1.2 Ag₂S-(2-Mercaptopropionic acid) Quantum Dots

Ag₂S is the core material while 2-MPA (2-mercaptpropionic acid) is the coating. Ag₂S is stable in alpha phase, and its band gap energy is 0.9 eV (Madelung, 2004). Previously, it was reported that bulk Ag₂S have no significant toxicity (Hirsch, 1998). Properties such as cytocompatibility, low energy band gap and near infrared region (NIR) emission make Ag₂S QDs a very convenient probe for biological applications (Yarema, 2011). 2-MPA (Fig. 1.21) is bound to crystal surface through thiol groups and is water soluble due to carboxylic acid units residing at the outer surface. Although the benefits of the isomer 3-MPA as a coating material for QDs has been investigated for some time, the application of 2-MPA is a relatively novel approach. In respect to 3-MPA, 2-MPA was found to be more effective in terms of

improved fluorescence signal and nanocrystal stability. Also, solubility of 2-MPA in water makes it possible to synthesize aqueous QDs. Water solubility of a QD enhances the biocompatibility. Aqueous synthesized QDs have higher colloidal stability and lower luminescence than the QDs synthesized in organic solvent (Fig 1.22) (Acar et al, 2009).

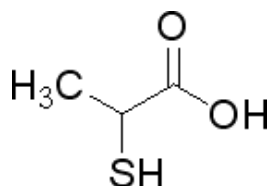


Fig 1.21 Chemical structure of the 2-MPA (Sigma Aldrich).

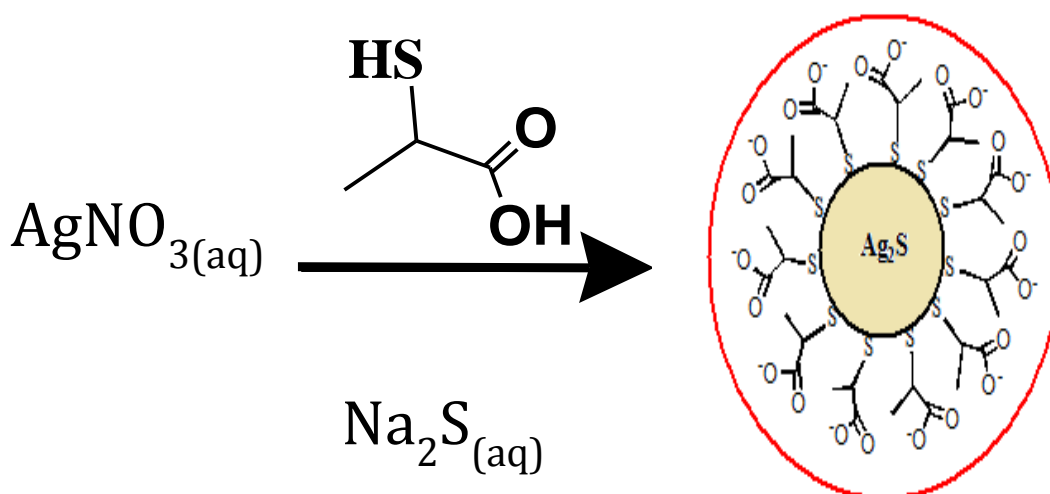


Fig 1.22 Aqueous synthesis of 2-MPA coated Ag_2S .

$\text{Ag}_2\text{S}/2\text{-MPA}$ QDs have an excitation maxima of 490 nm and an emission maxima of 830 nm at near infrared region (Fig. 1.23). The core size of the QD is determined as 3.72 nm while the hydrodynamic size of the QD in water is found to be 4.2 nm. Zeta potential of the nanocrystal is -59 mV. These nanoparticles were synthesized and physically characterized by İbrahim Hocaoğlu at Assoc. Prof. Dr. Funda Yağcı Acar's lab.

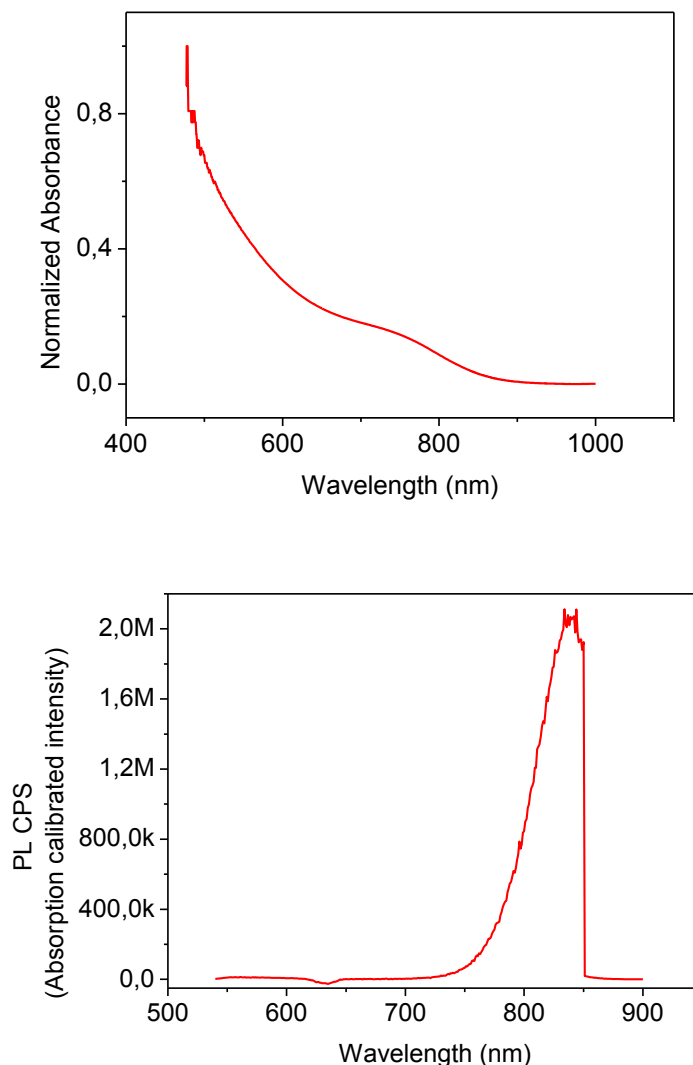


Fig 1.23 Excitation and emission spectra of $\text{Ag}_2\text{S}/2\text{-MPA}$ QDs.

1.3 Cell Viability Assay

XTT assay is a cell viability measurement method that depends on metabolic activity of the cell. This assay was chosen in order to determine whether QDs have a negative effect on cell's enzymatic activities.

XTT application as a viability assay was first suggested as a method to replace the MTT assay (Scudiero et al, 1988). XTT (Fig 1.24) is a more recent version of tetrazolium salt MTT. These salts both produce formazan when reduced by enzymes,

however XTT formazan is water soluble. Therefore XTT is much more preferable since MTT assay requires additional solubilization steps (Fig 1.25).

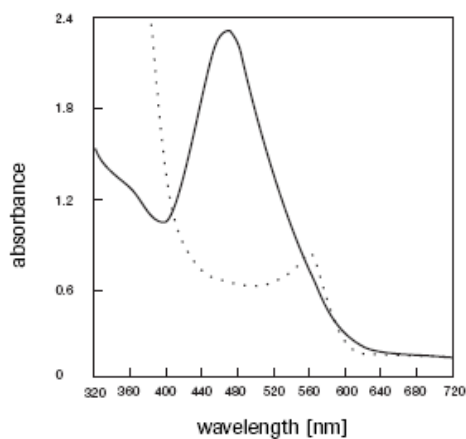


Fig 1.24 UV spectra of the XTT (dotted) and formazan (Roche, 2011).

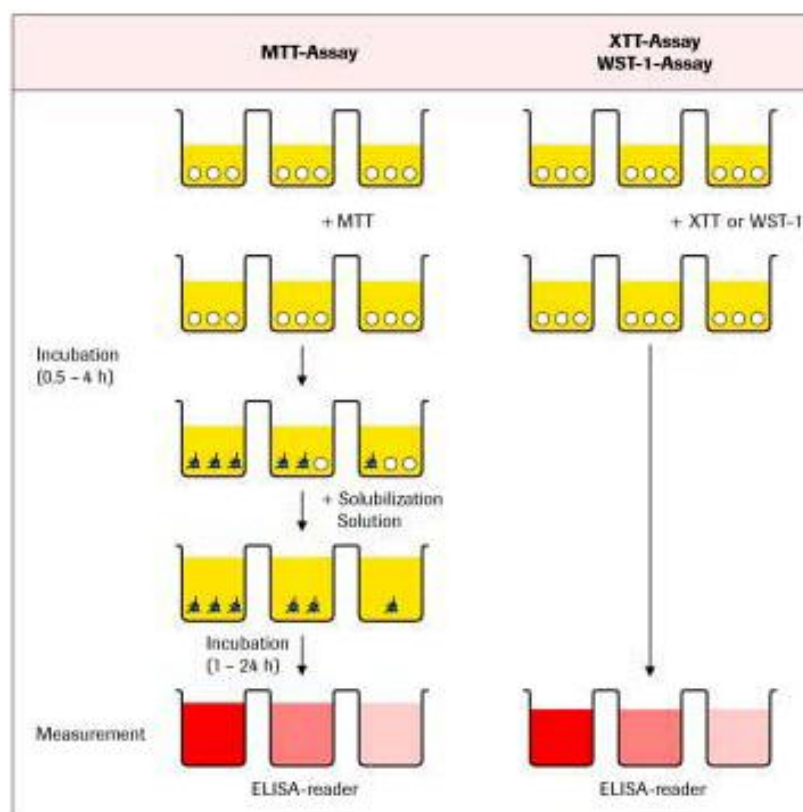


Fig 1.25 The differences of experiment procedures between MTT and XTT (Roche, 2008).

The cleavage of XTT takes place in mitochondria of viable cells which have reductase enzymes that forms formazan from tetrazolium salts (Fig 1.26). XTT is a yellow colored molecule but as more XTT is reduced to formazan the color would turn to orange since formazan is orange colored. Thus, darker color means higher metabolic activity. The difference in the color change is read in ELISA plate reader as absorbance. (Biological Industries, 1998).

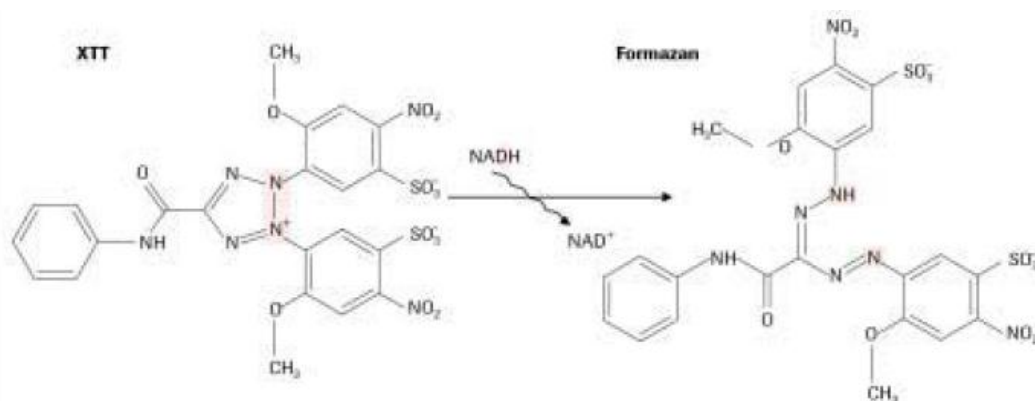


Fig 1.26 Cleavage of XTT which produces formazan (Roche, 2008).

1.4 CyQUANT® Cell Proliferation Assay

XTT assay measures viability by metabolic activity. Another kind of cell proliferation measuring method is based on DNA detection. These assays work by determining the used amount of the radioactive isotope tritiated thymidine (3H-TdR) in DNA synthesis or by the integration of 5-bromo-2'-deoxy-uridine (BrdU) to DNA (Roche, 2008).

Therefore, CyQUANT® cell proliferation assay was also used in cytotoxicity experiments in order to see QD's effect on nucleic acids. The fluorescent dye in this assay kit is called CyQUANT® GR (Fig 1.27) and it can bind to nucleic acids that come from lysed cells. When this dye is bound, a considerable increase in the fluorescence intensity is observed. The fluorescence produced by CyQUANT® GR and nucleic acid binding is measured with a microplate reader. Samples with more cells are expected to give higher fluorescence.

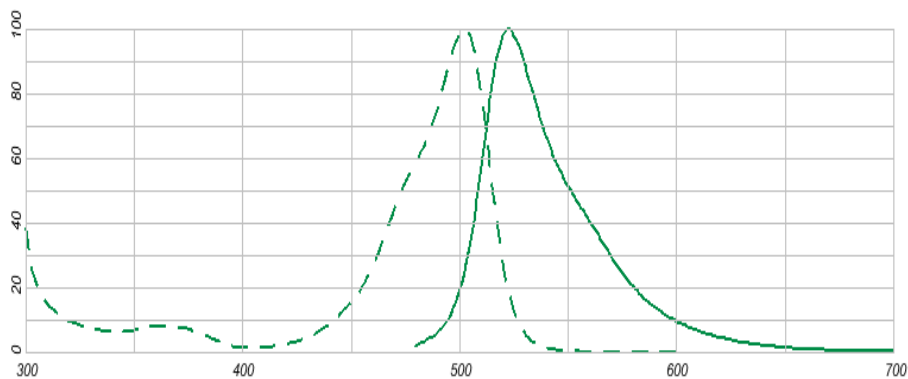


Fig 1.27 Spectrum of DNA bound CyQUANT GR dye (Fluorescence SpectraViewer, 2011)

This proliferation assay has a capacity of detecting 50 to 250,000 cells linearly. In addition to cell proliferation studies, other experiments such as determination of cell number, determination of DNA and RNA content and cell adhesion analysis can be conducted with this kit. It is also compatible with a large range of cell types and investigations performed on mouse fibroblast cells, canine kidney cells have already been reported (Invitrogen, 2006). CyQUANT[®] cell proliferation assay was also used in studies for endothelial cell alignment throughout blood vessel formation (Hoang et al, 2004).

1.5 Confocal Laser Scanning Microscopy

Microscopy studies give an idea about the localization and distribution of QDs in cells.

A confocal laser scanning microscope is a very convenient tool for QD imaging with its ability to control depth of field and to eliminate the background noise from the focal plane. Pinhole apertures which are located in front of the laser excitation source and the photomultiplier detector create a conjugate plane (confocal) (Fig 1.28). Therefore, out-of focus light or glare will be reduced to give more defined images of the selected section (Fig 1.29). This property of confocal laser scanning microscopy enables the scientist to take 0.5 to 1.5 micrometer of optical sections from the specimen without the hassle of physical sectioning (1.30) (Claxton et al, 2006).

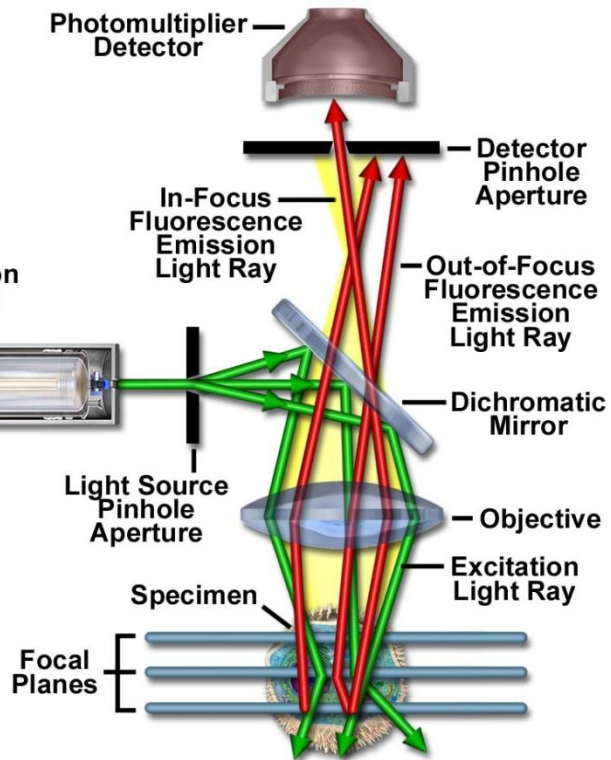


Fig 1.28 Diagram showing optical pathway and basic apparatus of CLSM (Claxton et al, 2006).

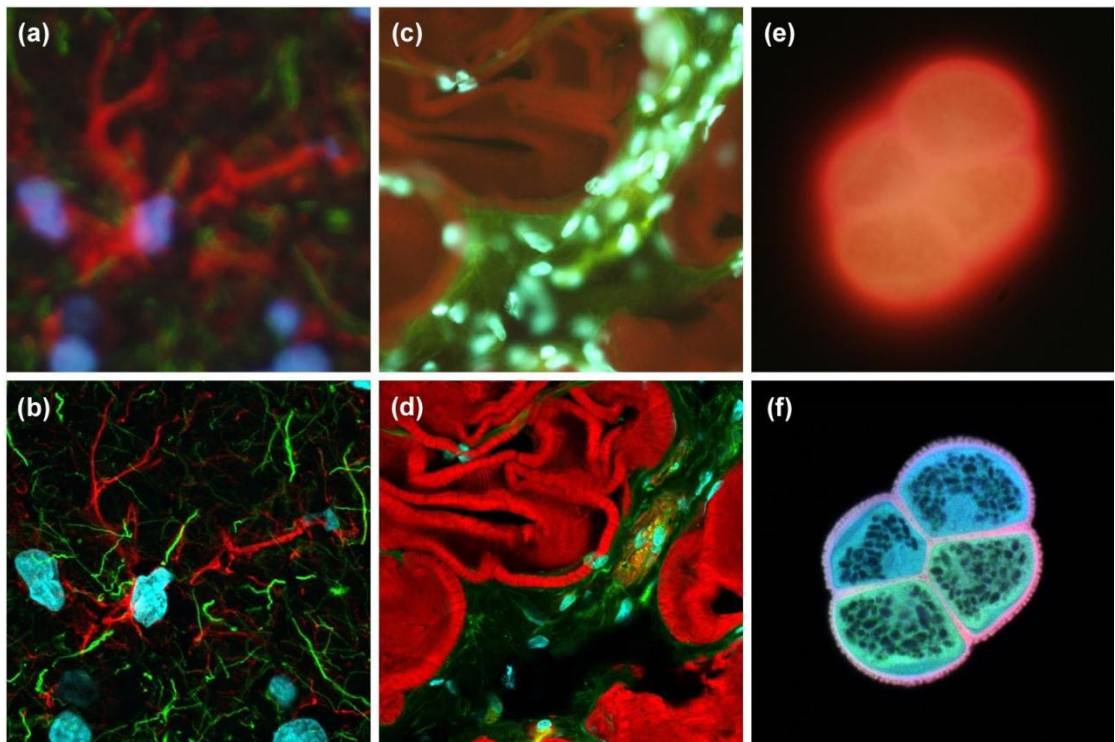


Fig 1.29 Comparison of widefield microscopy (upper row) to confocal laser

scanning microscopy (lower row) images. (a) and (b) are the images of mouse brain hippocampus, (c) and (d) are from rat smooth muscle, (e) and (f) sunflower pollen grain tetrad (Claxton et al, 2006).

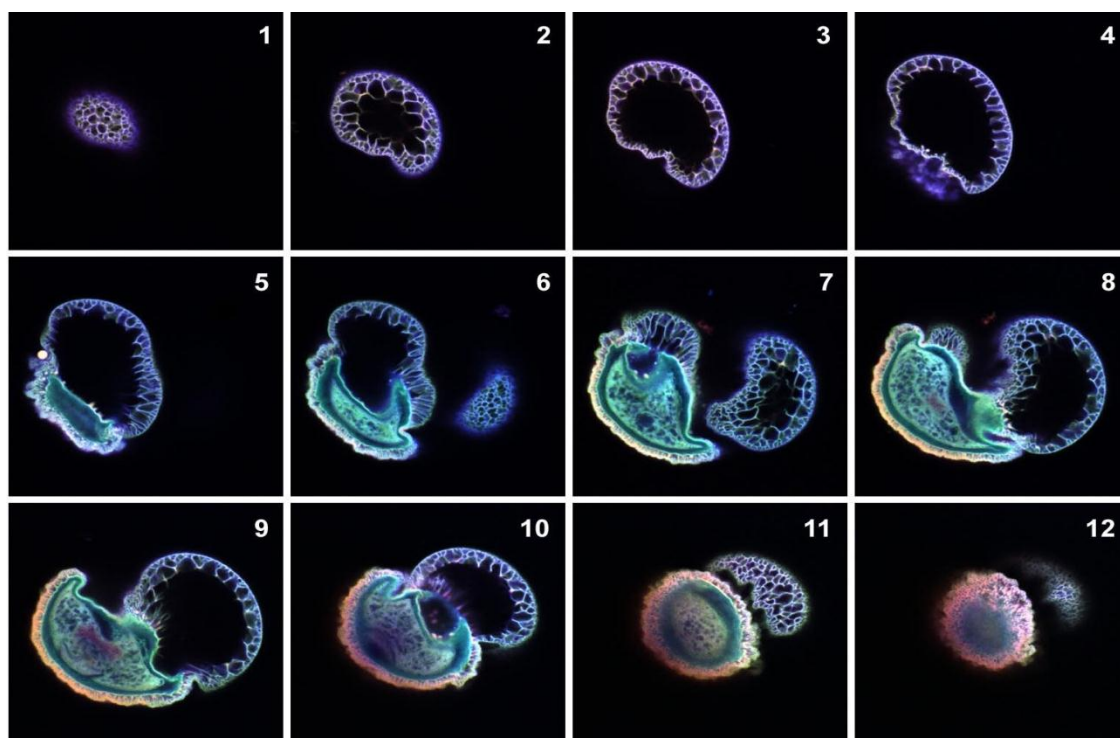


Fig 1.30 Optical sections of lodgepole pine (*Pinus contorta*) pollen grain (Claxton et al, 2006).

1.6 Uptake Assay: Quantitative Determination of Internalization

Confocal scanning microscopy is used to demonstrate the internalization of QDs by the cells. However, this method cannot suggest any information on the effect of QD concentration on uptake rate and amount, in other words internalization efficiency. Also, internalization is a process which is affected by factors such as temperature and coating material (Ryman-Rasmussen et al, 2007). Therefore, emission intensity of QD treated cells are measured by a microplate reader and a quantitative value such as QD concentration is assigned to these fluorescence values by the integration of a calibration curve.

1.7 Apoptosis Analysis

Apoptosis analysis with an annexin V based assay can give healthy and necrotic cell numbers as well as the apoptosis percentage of the sample. After conducting the initial cytocompatibility studies with XTT and CyQUANT[®], we also wanted to determine whether Ag₂S-2MPA QDs cause any apoptotic behavior.

1.7.1 Working Principle

Living, necrotic and apoptotic cells can be detected with the annexin based apoptosis assay (Agilent Technologies, 2003). This apoptosis assay works with two fluorescent dyes, calcein AM and Cy5 (Fig 1.31).

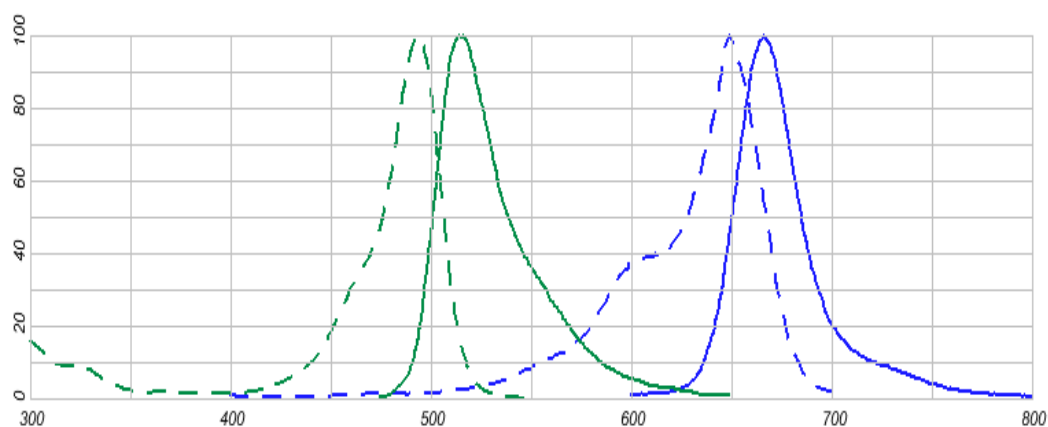


Fig 1.31 Ex (dotted) and em spectra of the calcein AM (green) and cy5 (blue) (Fluorescence SpectraViewer, 2011)

Calcein acetyloxymethyl (AM) is a green fluorescence probe that can enter both live and dead cells. Its cleavage by the intracellular esterases forms calcein which emits the green fluorescence. Cells with intact membranes keep calcein inside the cell. Since, in the stage of early apoptosis, cell membrane is not yet disintegrated, calcein does not leak from the cell and therefore can stain apoptotic cells as well as healthy cells. However, cells with leaky membrane, necrotic and late apoptotic cells, lose calcein and cannot emit green fluorescence (Agilent Technologies, 2001).

Cy5 is the second dye and it emits red fluorescence. Streptavidin labeled Cy5 is used in this apoptosis assay because it is bound to biotin conjugated annexin V. Annexin V is the detector of apoptosis and necrosis.

In the early stages of apoptosis and necrosis phosphatidyl serine (PS), an inner-leaflet component of the cell membrane, translocates to the external surface of the cell. Annexin V is a calcium and phospholipid binding protein which has a high affinity for PS. When annexin V conjugated Cy5 binds to PS, the cell membrane starts to emit red fluorescence. Therefore, stained apoptotic cells emit green fluorescence from the cytoplasm and red fluorescence from the membrane, whereas healthy cells can only be stained with Calcein AM which emits green fluorescence. Since necrotic cells have compromised membranes, they cannot retain Calcein AM inside but their membrane can be stained with Cy5 (Fig. 1.32).

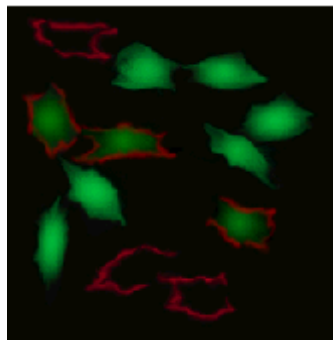


Fig 1.32 A representative image for the annexin V conjugated Cy5 (red) and calcein (green) based staining for apoptosis detection (Agilent Technologies, 2003). Green cells are healthy, green cells with red membranes are apoptotic and cells which have only red membranes are necrotic.

1.7.2 Microfluidic Cell Chips

Agilent 2100 Bioanalyzer cell chip assays work as basic flow cytometric analysis. The chips work not with an electrode cartridge as nucleic acid and protein assays but with a pressure cartridge. Samples are loaded to these microfluidic chips and chip can hold 6 samples (Fig 1.33). With the flow of the cell buffer, cells are aligned as a

line and fluorescence of the every single cell is measured (Fig 1.34) (Agilent Technologies, 2003).

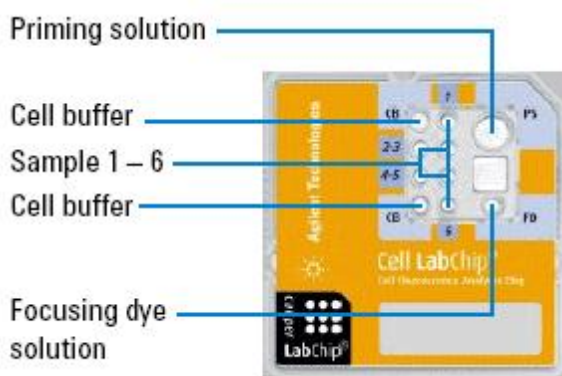


Fig 1.33 Solutions and their placements on the chip (Agilent Technologies, 2003).

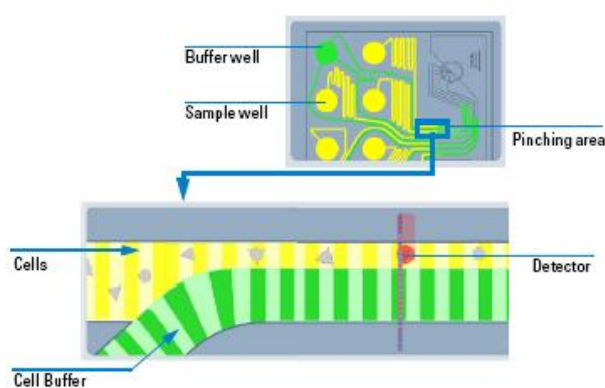


Fig 1.34 Diagram of the microfluidic system (Agilent Technologies, 2003).

Agilent 2100 Bioanalyzer can detect two colors of fluorescence. The red laser diode emits highest at 635 nm and the blue LED emits highest at 470 nm. Detection range of the channels are 674 to 696 nm and 510 to 540 nm, respectively.

1.8 Aim of the Study

Desirable optical properties of quantum dots make them effective cell imaging probes as well as targeting and drug delivery platforms. However, a quantum dot must also have low cytotoxicity and high cellular uptake to be considered suitable for such applications.

The aim of this study was in vitro characterization of Ag₂S-2MPA quantum dot to evaluate its potential in biological applications. For this purpose, we have used various microscopic and spectroscopic methods to study cytotoxicity, uptake and intracellular localization of the particles. A wide QD concentration range (10-600 ug/mL) was tested on NIH/3T3 mouse fibroblast cell line. For qualitative uptake, localization and morphological assessment, confocal laser scanning microscopy was used. XTT metabolic activity and CyQUANT[®] cell proliferation assays were used as indicators of the cell viability. An Annexin V based cell assay was also included in the study to differentiate between cell necrosis and apoptosis.

CHAPTER 2

EXPERIMENTAL

2.1 Materials

2.1.1 Cell Lines

NIH/3T3 mouse embryonic fibroblast (Şap Institute, Turkey) cell line was a gift from Assist. Prof. Dr. Elif Erson Bensen, Middle East Technical University Biological Sciences Department.

2.1.2 Chemicals & Reagents

Etoposide “Ebewe” was produced by Ebewe Pharma (Austria). All cell treatments were done by the use of a sterile 50 mg/2.5 mL Etoposide solution.

Dulbecco's Modified Eagle's Medium (DMEM) (Table A.1), FBS and trypsin-EDTA in PBS without calcium and magnesium were purchased from Biochrom AG, Germany. Pen-Strep (Penicillin-Streptomycin) was acquired from Thermo Fisher Scientific, USA. XTT Cell Proliferation Kit was purchased from Biological Industries, Israel. CyQUANT® Cell Proliferation Assay Kit is a product of Invitrogen, USA. Trypan blue solution (0.4%) comes from Sigma, USA. Paraformaldehyde powder was obtained from Merck, Germany. Annexin V-Biotin Apoptosis Detection Kit was purchased from Oncogene Research Products, USA. Fluorolink Cy5 labeled streptavidin was acquired from Amersham, USA. Calcein-AM was purchased from Molecular Probes, USA.

2.1.3 Ag₂S-(2-mercaptopropionic acid) Quantum Dots

Ag₂S core with 2MPA polymer coating QD was produced by Assist. Prof. Dr. Funda Yağcı Acar, Koç University, Istanbul, Turkey.

2.2 Methods

2.2.1 Cell Culture

2.2.1.1 Cell Culture Conditions

NIH/3T3 cells were cultured in DMEM (Appendix A). Medium was supplemented with 10% (v/v) FBS and 1% (v/v) Pen-Strep (This type of medium is referred as the complete medium from now on). Cell culturing was conducted in T-25, T-75 and T-175 tissue culture flasks (Greiner Bio-One, Germany). All incubations were carried out at 37^oC in Sanyo (UK) incubator with humidified and 5% (v/v) CO₂ contained air.

2.2.1.2 Subculturing

Cells were always subcultured after reaching 80% confluency on the flask surface. In the process of subculturing, existing medium was replaced with PBS in order to wash away any remaining serum since the presence of serum inactivates trypsin. Cells were detached with 5 minutes trypsinization at 37^oC. Complete medium was added after trypsin treatment. The cell suspension was divided and transferred into new flasks and more complete medium was added until the flask bottom was covered.

2.2.1.3 Cell Stock Preparation

3 mL complete medium was added onto a detached cell solution in 3 mL trypsin in order to inactivate trypsin. After mixing thoroughly, 6 mL cell suspension was divided into two 15 mL falcons (Greiner Bio-One, Germany) and centrifuged (Sartorius,

Sigma, USA) at 100 g for 10 minutes. The resulting supernatant was aspirated and the cell pellet was resuspended in 1 mL ice cold complete medium which contained 5% (v/v) filter sterilized DMSO. These 1 mL cell suspensions were transferred into cryovials (Greiner Bio-One, Germany) and frozen at -80°C overnight. Frozen stocks were placed in liquid nitrogen the next day.

2.2.1.4 Stock Thawing

For thawing, 1 mL complete medium at 37°C was added to the frozen cell stock solution. The thawed cell suspension was then transferred to a T-25 flask which contained 4 mL complete medium at 37°C .

2.2.1.5 Viable Cell Count With Trypan Blue

Cells that have damaged membranes, i.e. dead cells, can be stained with negatively charged Trypan Blue dye (Freshney *et al.*, 1987). Since, live cells that have intact membranes can actively expel trypan blue, only dead cells can be stained blue.

Diluted cell suspension was stained with the trypan blue solution which was added in 1:1 ratio. After two minutes incubation with trypan blue, a Neubauer hemacytometer (Superior, Germany) was used to count the cells with a phase contrast microscope.

Unstained cells that reside in the 64 large squares and 25 small squares of the hemacytometer were counted and the cell number was multiplied with the dilution factor and 1000 to find the number of cells in 1 mL cell suspension.

2.2.2 Spectral Analysis of the Quantum Dots

Spectral properties of the QD were required for in-vitro imaging and uptake assay. Excitation and emission scan of QDs were obtained with a microplate reader (SpectraMax, USA). QD solution concentration was 1.32 mg/mL. Wavelength

settings were adjusted according to the information given by Acar Lab.

Table 2.1 Excitation scan wavelength settings

| QD Composition | Excitation (nm) | Emission Range (nm) |
|------------------------|------------------------|----------------------------|
| Ag ₂ S-2MPA | 400 | 790 - 840 |

2.2.3 XTT Assay

Effect of QD treatment on cell viability was measured with XTT assay. XTT, which is a normally yellow colored tetrazolium salt, can be converted to orange colored formazan by reduction in metabolically active cells. Resulting variation in color, which would be more distinct in more metabolically active samples, can be detected with absorbance reading (Biological Industries, 1998).

10,000 cells per well were seeded into 96-well plates and were incubated overnight (at 37°C, under 5% CO₂). The next day, cells were treated with QD included complete medium and incubated another 24 hours. When the incubation period was over, medium with QD was discarded and each well was washed with complete medium and 90 µL working solution (30 µL XTT reaction solution and 60 µL medium) was added. Samples were left to incubation for 2 hours.

Spectromax 340 96 well plate reader (Molecular Devices, USA) was used for absorbance reading at 500 nm. Any undesired absorbance reading which is caused by cell debris, fingerprints etc. was excluded from 500 nm reading by taking another reading at 650 nm. The absorbance value of 650 nm was subtracted from the value of 500 nm. Working solution was used as blank.

2.2.4 Proliferation Assay

The CyQUANT[®] Cell Proliferation Assay Kit (Invitrogen, USA) uses a green fluorescent dye called CyQUANT[®] GR that emits strong fluorescence at 520 nm when bound to cellular nucleic acids. The assay kit also contains a cell-lysis buffer

which is more efficient when cells are frozen and thawed prior to the application.

The cells were seeded to a 96-well plate (Greiner Bio-one, Germany), each well containing 10,000 cells. This step was followed by an overnight incubation period (at 37°C, under 5% CO₂) for the attachment of the cells to the well bottom. In the morning, complete medium in the wells was changed with QD containing complete medium. After an incubation (at 37°C, under 5% CO₂) for 24 hours, medium with the remaining extracellular QD was aspirated and wells were washed once with 200 µL PBS to remove the phenol red residue that is left from the medium. The cells were then frozen at -80 °C. Just before fluorescence reading, cell pellet was thawed at room temperature and 200 µL CyQUANT[®] GR dye/cell-lysis buffer was added to each well. All samples were prepared as triplicates and CyQUANT[®] GR dye/cell-lysis buffer solution was used as blank cell-lysis blank.

For the preparation of the calibration curve, a cell suspension of 10⁶ cells in complete medium was centrifuged (5 min, 200 x g). The cell pellet was resuspended in 1 mL PBS and then centrifuged (5 min, 200 x g) again. Supernatant was discarded and the cell pellet was frozen at -80 °C. For the fluorescence reading, cell pellet was thawed at room temperature and 1 mL CyQUANT[®] GR dye/cell-lysis buffer was added. A dilution series in terms of cell number was prepared in the wells of a 96-well plate. Cell number range was from 30,000 to 250,000 cells per well. Our control was CyQUANT[®] GR dye/cell-lysis buffer without any cells and our blank was cell-lysis buffer itself. All samples were prepared as triplicates. Linear regression plot was generated in GraphPad Prism 5 Software.

2.2.5 Fixed Cell Imaging

Cells were seeded into a 6-well plate which has autoclaved coverslips (Marienfeld, Germany) in its wells. The cell number in each well was set to 50000 in 2 mL complete medium. After an overnight incubation (at 37°C, under 5% CO₂), cells were treated with QD containing complete medium. After the QD incubation period was completed, medium was aspirated and wells were washed with 2 mL PBS. Cells

that have grown on the coverslips were fixed with 1.5 mL 4% (w/v) paraformaldehyde solution for 10 minutes at room temperature. Fixation was followed with two PBS washes. Coverslips were taken out of wells, inverted and mounted on slides. PBS was used as the mounting medium. Imaging was performed on Zeiss LSM 510 confocal laser scanning microscope (Jena, Germany).

For evaluation of the QD on cell morphology phase contrast transmission mode is used with the LD A-Plan 20X/0,30 Ph1 lens. In order to observe the intracellular localization of the QDs fluorescence imaging was performed. Widefield fluorescence images were taken using Plan-Neofluar 40X/1.3 Oil DIC lens with DAPI and GFP filter and mercury arc lamp. For confocal imaging argon laser (458 nm - 488 nm) and HeNe1 laser (543 nm) was applied with Plan-Neofluar 40X/1.3 Oil DIC lens. During confocal imaging settings were adjusted to the 1 airy unit, 1024 X 1024 pixels and 12 bit images were taken by using the same laser power and detector sensitivity for each image.

2.2.6 Uptake Assay

In this experiment, QD treated cells are used for fluorescence readings at excitation and emission wavelengths suitable to the QD's spectral properties. Fluorescence intensity values obtained from this reading are then converted to QD concentration values by the use of a calibration curve. This QD concentration gives the amount of QD internalized by cells via endocytosis.

The cells were seeded to a T-75 flask. After 80% confluency was reached, complete medium was changed with QD containing complete medium. After an incubation period of 24 hours, medium with the remaining extracellular QD was aspirated and cells were detached by 3 mL trypsin-EDTA. Before adding trypsin-EDTA, cells were washed with PBS to remove any remaining serum. When the detachment of the cells is confirmed with microscopic observation, complete medium was added in 1:1 ratio in order to inactivate the trypsin enzyme. Cell suspension was transferred to a sterile 15 mL falcon tube. A small amount of cell suspension was used for cell count with

hematocytometer. Both live and dead cells were included to the count. Cell number differences between each sample was corrected by selecting a certain number of cells. Samples were centrifuged and supernatant was discarded. Cells were resuspended in 1X PBS and transferred to a 96 well plate.

Fluorescence readings were taken with the same settings used at calibration curve preparation. Internalized QD amount by total cells were found using the calibration curve equation and QD uptake per cell was determined using the results obtained at hematocytometer count by dividing the total internalized QD amount value to cell number.

2.2.7 Annexin V Based Apoptosis Assay

2.2.7.1 Sample Preparation

80% confluent cells at T75 flasks were subcultured to the T175 flask and they were incubated for 24 hours. Cells were incubated for 24 hours. Medium was collected from each flask to separate 50 mL falcon (Greiner Bio-One, Germany). Cells were washed with 10 mL 1X PBS and PBS was collected to the corresponding falcon. Cells were trypsinized with 5 mL trypsin-EDTA and after cells were detached 5 mL full medium was added. Detached cells were collected to the corresponding falcon tubes. Cells were counted using hematocytometer. 1×10^6 cells were transferred to another falcon and they were centrifuged at 400 g for 5 minutes. Supernatant was discarded. QD fluorescence effect on bioanalyzer measurement was tested by preparing a sample from QD applied cells and resuspending the cells in 500 μ L cell buffer. For staining the samples, cells were resuspended in 1 mL medium. 20 μ L media binding reagent and 2.5 μ L annexin V-biotin were added to the each sample and cells were incubated for 15 minutes at room temperature (Fig. 2.1). Samples were centrifuged at 400 g for 4 minutes. Supernatant was discarded and cells were resuspended with 1 mL 1X binding buffer. 2 μ L Cy5-streptavidin and 1 μ L calcein were added to the samples and they were incubated at room temperature for 10 minutes. Cells were washed with 1 mL 1X binding buffer and resuspended in 500 μ L

cell buffer. From each sample 10 μL was loaded to the chip and chip was inserted to the Agilent 2100 Bioanalyzer (Agilent Technologies, USA).

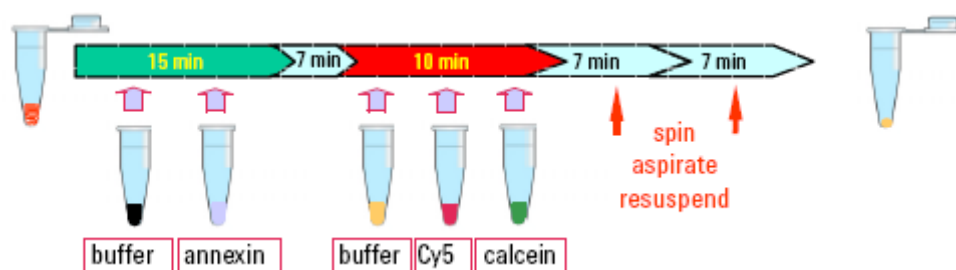


Fig 2.1 Diagram for apoptosis staining (Agilent Technologies, 2002)

2.2.7.2 Chip Loading and Running

Each chip can hold 6 samples. Sample loading volume is 10 μL which contains approximately 20,000 since the final concentration of the sample should be 2×10^6 cells per mL.

The Agilent 2100 bioanalyzer measures the fluorescence coming from the stained cells and it has two channels: Blue and Red. Blue channel detects from 510 to 540 nm and red channel detects from 674 to 696 nm. Calcein AM is detected by the blue channel and Cy5 is detected by the red channel. For excitation of these probes, there is two lasers: The blue LED emits highest at 470 nm and the red laser diode emits highest at 635 nm.

2.2.7.3 Data Analysis

A pre-optimized program called Apoptosis Series II was selected in order to read the fluorescence intensities. Every cell is measured and if the read fluorescence intensity value is higher than the predetermined intensity value, the cell is assigned as an event.

Total cell number for each sample is given as “the total event number” and cells that gives either red or green fluorescence are represented as “gated event number” in

histogram charts. The dot plot chart displays the number of events that are gated by both red and blue channel.

If gated event numbers for each staining type were given names such as;

- i. Red channel (all red emitting events) = R
- ii. Blue channel (all green emitting events) = B
- iii. Both channels (both red and green emitting events) = BR

Then;

- Number of healthy cells = $B - BR$
- Number of necrotic cells = $R - BR$
- Number of apoptotic cells = BR

2.2.8 Statistical Analysis

Statistical analysis was performed for the XTT, cell proliferation and cadmium assays. All data were presented as mean \pm SEM. Statistical evaluation was performed with GraphPad Prism Software (GraphPad Software, Inc., USA). One way ANOVA test was applied and for comparing columns as pairs Tukey's multiple comparison test was chosen. Differences were expressed as significant at $P < 0,05$.

CHAPTER 3

RESULTS AND DISCUSSION

3.1 Cytocompatibility

As discussed earlier, quantum dots possess many qualities that are advantageous over traditional organic dyes. Therefore, the use of the quantum dots as fluorescent probes in biological applications is becoming more prominent. However, since they have a cytotoxic chemical structure, they need to be investigated for any negative effects. In this study, we adopted two cytotoxicity assays which measure the cellular health state by two different approaches.

3.1.1 Metabolic Activity Determination with XTT Assay

XTT assay is a widely used method for the indirect assessment of cytotoxicity. It measures the metabolic activity rate via enzymatic processes. The XTT reagent which is the key element of this assay is cleaved by mitochondrial reductase enzymes and the product is an orange colored molecule which is called formazan. The amount of the color change in the cell culture is higher when the cells are metabolically active. A spectrophotometer can detect small color changes as an absorbance value.

3.1.1.1 Assay Optimization

The application parameters of the assay were optimized in terms of the amount of XTT reaction solution and the incubation time. The effect of phenol red presence in the medium was also investigated.

It was found that 30 μ L XTT reaction solution was sufficient to stain one well of cells (Fig 3.1). Absorbance values taken through time showed that two hours of

incubation time rests within the linear range (Fig. 3.2). Finally, another optimization experiment suggested no significant effect of phenol red presence (Fig. 3.3)

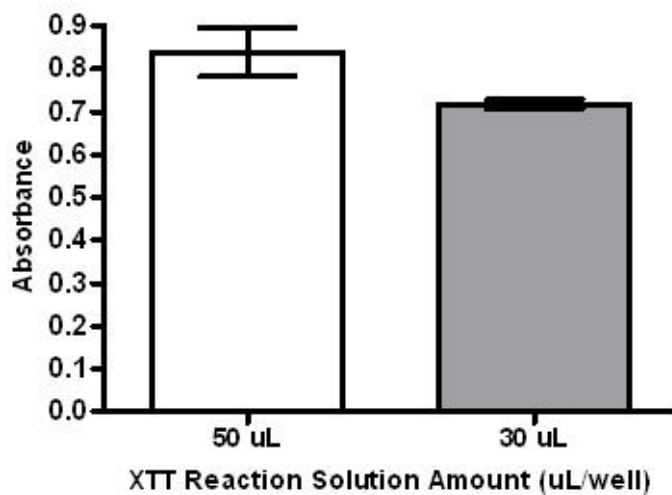


Fig 3.1 Optimization of XTT reaction solution volume.

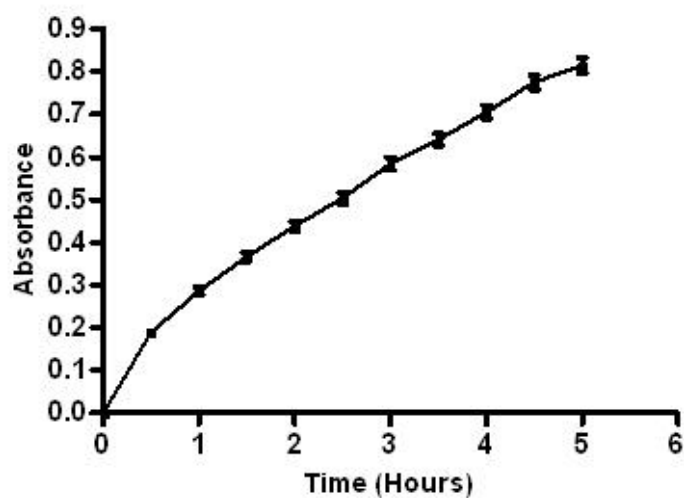


Fig 3.2 Optimization of XTT reagent incubation time for NIH/3T3 cells.

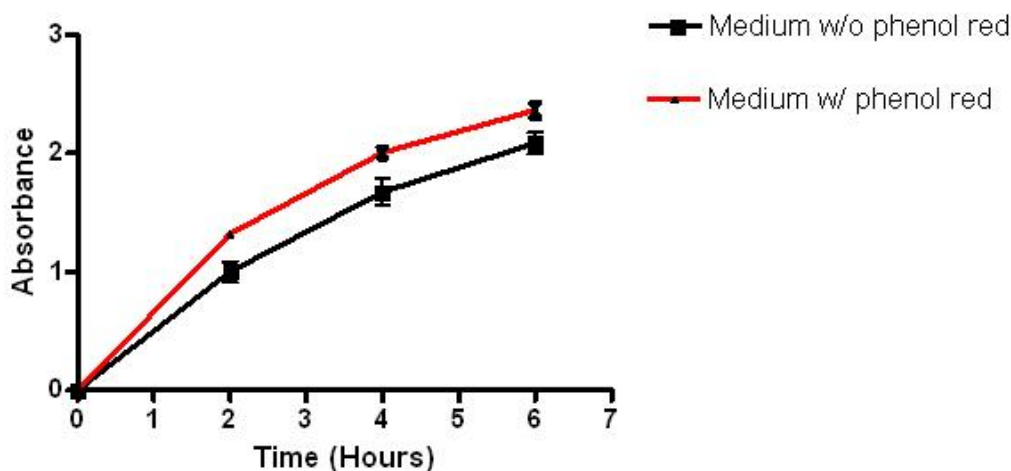


Fig 3.3 The absorbance difference between medium with and without phenol red.

3.1.1.2 Variation in the Metabolic Activity

NIH/3T3 cells were treated with various concentrations (10 to 600 $\mu\text{g}/\text{mL}$) of QD for 24 hours. Statistical analysis of the results indicates no significant difference in the vitality of untreated and $\text{Ag}_2\text{S}/2\text{-MPA}$ treated samples (Fig. 3.4).

When these results were compared with the XTT results of another QD that was synthesized by our group and consisted of CdS core and 2-MPA coating, it can be seen that Ag_2S core is extremely biocompatible. Because it was shown that CdS/2-MPA QD presence had dropped the metabolic activity rate by approx. 50% even in the treatment with a concentration as low as 25 $\mu\text{g}/\text{mL}$. Therefore, it can be said that the heavy metal cadmium demonstrates high cytotoxicity even with coating. In addition, the coating itself seems to have no additional effect of toxicity since it was also used on Ag_2S QDs. Absence of significant metabolic activity decrease with Ag_2S core is in correlation with preceding studies stating low or no toxicity for silver complexes unlike free silver ions (Suresh et al, 2011).

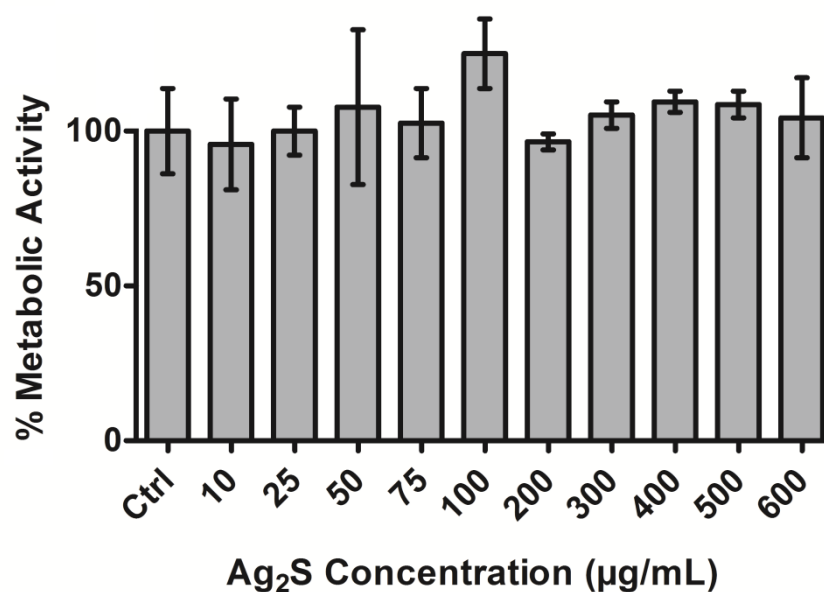


Fig 3.4 XTT results of QD treatments with various concentrations in NIH/3T3 cells after 24 hours of incubation. Reported values are mean \pm SEM.

3.1.2 Nucleic Acid Content Determination with Proliferation Assay

XTT is a cell viability assay which measures the metabolic activity rate of the cell through enzyme activity. As presented in the previous section, Ag₂S quantum dots were found to have no significant effect on enzymatic processes of the cell. It was previously reported that QDs can alter the oxidation-reduction reactions (Cooper et al, 2010). This effect may produce altered and thus, unrepresentative results. In consideration of these risks, we decided to conduct one more cytocompatibility experiment which would measure a different activity in the cell.

CyQUANT proliferation assay was chosen as the secondary cytotoxicity measurement utility since it works by measuring the nucleic acid content. This assay includes a dye which is highly fluorescent when bound to nucleic acids. This fluorescent signal's intensity can be measured by a microplate reader where higher intensity would mean more cells, and therefore, a higher rate of proliferation.

3.1.2.1 Standard Curve for Cell Number

In order to convert fluorescence intensity values to cell amount, a calibration curve was prepared from seven dyed cell suspensions that contained cells between 50 to 50,000. This range was chosen because CyQUANT proliferation assay can linearly detect 50 to 50,000 cells. The best fit formula ($y = 0.04x + 94.67$) was generated for the calibration curve in which y represented RFU values and x represented cell number. The goodness of fit was found to be 0.9573 (Fig 3.5).

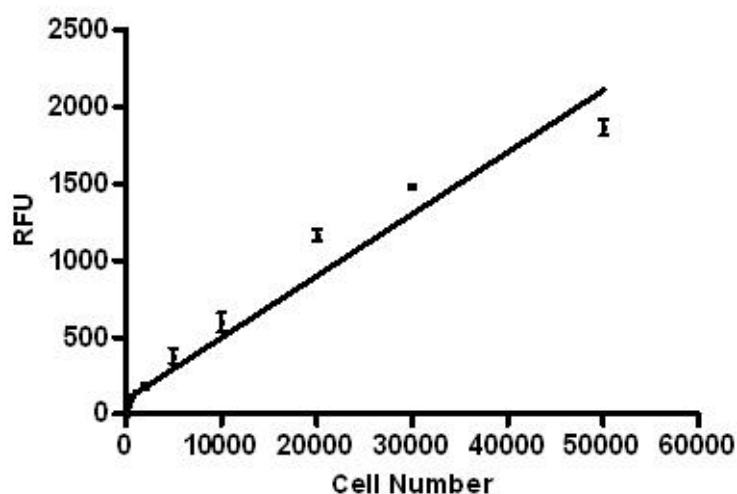


Fig 3.5 Standard curve for the proliferation assay of NIH/3T3 cells.

3.1.2.2 Variation in Cell Proliferation

NIH/3T3 cells were treated with five different concentrations of QD, ranging from 75 $\mu\text{g/mL}$ to 400 $\mu\text{g/mL}$ for 24 hours. This incubation period was then followed by the assay application and the fluorescence signal was read on the microplate reader. All RFU values were converted to cell numbers by the use of the best fit formula of the standard curve. All samples were prepared as triplicates and the negative control was untreated cell samples. There were also another set of controls which consisted of QD treated but not stained cells. These were included in case of any unwanted QD excitation during the reading of the samples. The RFU read from these samples were to be subtracted from the actual samples' RFU values. However, it was

observed that these samples were not excited enough with the microplate reader settings of this experiment to emit a significant fluorescence.

Although there seems to be a decrease (Fig. 3.6) in cell number with increasing QD concentration, observed differences are within experimental error interval. Therefore, AgS quantum dots seem to have no effect on cell proliferation, as well as on metabolic activity.

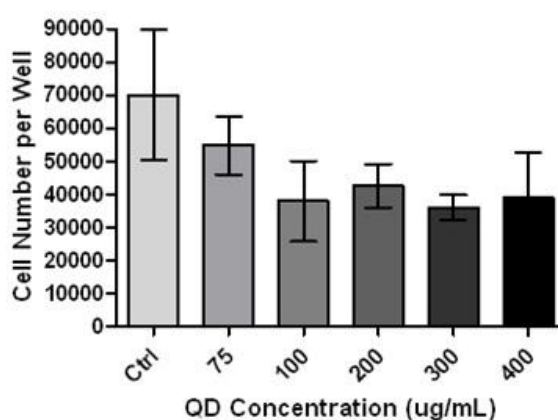


Fig 3.6 Proliferation assay results of QD treatments with various concentrations in NIH/3T3 cells after 24 hours of incubation. Reported values are mean \pm SEM (n=3).

3.2 Cellular Internalization and Localization

3.2.1 Cell Imaging

Cytocompatibility studies showed that Ag₂S QDs are highly suitable for imaging and targeting applications since it was observed that, even at the highest concentrations, it does not have any negative effect on cell metabolism. Therefore it was of the essence to study the the treatment efficiency in terms of internalization amount and intracellular localization of these QDs. In vitro imaging studies were conducted as a qualitative measurement tool.

NIH/3T3 cells were seeded into wells that contained coverslips at the bottom and

treated with 200 $\mu\text{g}/\text{mL}$ QD for 24 hours. The coverslips on to which the cell were attached were then taken out of the wells and mounted to slides. Cells were fixed with 4% paraformaldehyde prior to mounting. LSM 510 confocal laser scanning microscope (Jena, Germany) was used for imaging.

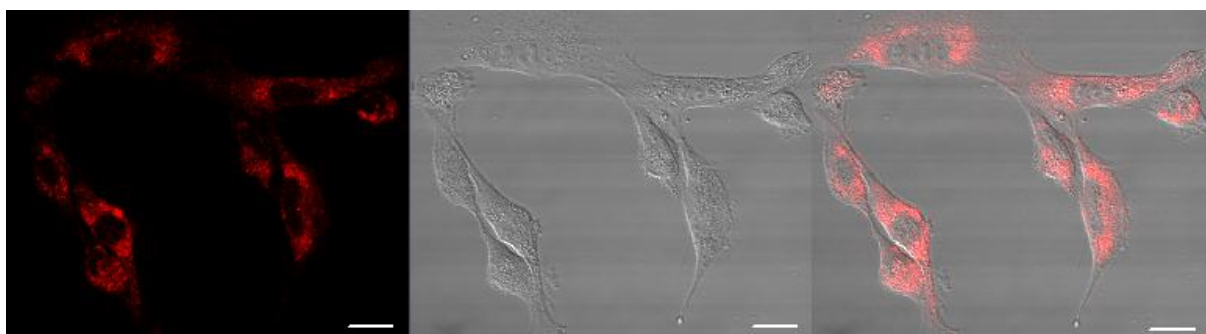


Fig 3.7 CLSM images of NIH/3T3 cells treated with 200 $\mu\text{g}/\text{mL}$ QD for 24 hrs. The scale bar represents 10 μm .

Internalization was successful while QDs displayed a punctuated cytoplasmic distribution (Fig. 3.7) which suggests confinement in endosomes and lysosomes as common for QD nanoparticles (Alivisatos et al, 2005).

Phase contrast transmission images showed that QD treatment at a concentration of 200 $\mu\text{g}/\text{mL}$ did not have adverse effects on the cell morphology, cell size and nucleus shape and these observations correlate with the XTT results.

Infra-red emission of the particles provides a major advantage in the cell imaging studies. Autofluorescence of cells is particularly strong in the green region of the electromagnetic spectrum. Therefore infra-red fluorescence imaging is ideal since there is minimal or no background signal from the cells in this region. However, typical confocal fluorescence Photo Multiplier Tube (PMT) detectors have low sensitivity in this region resulting in reduced photon collection. To overcome this difficulty, we increased the laser power and detector sensitivity to maximum allowed in our system. Using these settings, we could obtain high quality confocal images with a clean background.

Ag₂S QD emits at near infrared region. While this property eliminates the unnecessary background noise of autofluorescence which it is actually emitted near green region of light spectrum, it also makes it challenging to detect the QD fluorescence because confocal laser scanning microscope photomultiplier detector has a low sensitivity for infrared signals. However, since the cytocompatibility of the QD is quite high at this concentration, Ag₂S is still suitable for imaging and targeting studies.

3.2.2 Quantification of Uptake

Confocal microscopy studies demonstrated that Ag₂S QDs can be internalized by NIH/3T3 cells. Since imaging is a semi-quantitative method, another uptake measuring application was incorporated to our characterization studies. With this secondary experiment, it is possible to convert the fluorescence intensity to QD concentration.

For this purpose, cells that were treated with a certain QD concentration were read for QD fluorescence on the microplate reader.

This method was first optimized on Qdot 565 ITK Carboxyl Quantum Dot which is a commercial QD from Invitrogen.

3.2.2.1 Optimization Studies

A series of experiments were conducted in order to determine the fluorescence reading solution and the number of seeded cells per sample. It was found that complete medium had its own fluorescence interfering with the reading. When the medium was removed and cells were resuspended in PBS, background noise was significantly diminished (Fig 3.8).

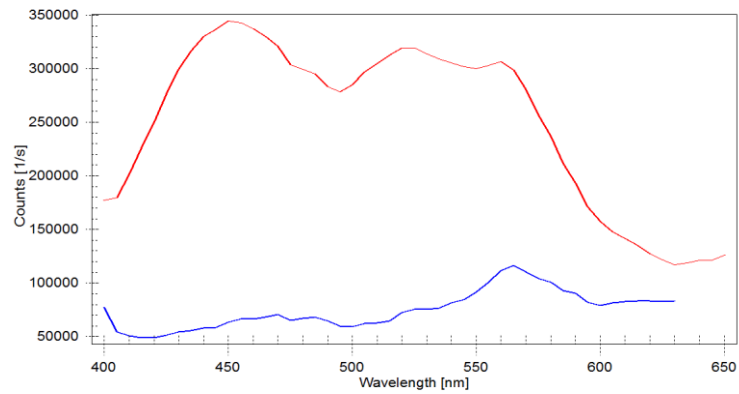


Fig 3.8 Fluorescence scan of 0.16 nM Qdot 565 ITK Carboxyl in complete medium (red) and in PBS (blue).

Seeding of 50,000 cells per sample was found to be insufficient since the treated sample fluorescence intensities were not very different from untreated samples (Fig 3.9). It was observed that QD internalized by 50,000 cells was not enough to emit significant fluorescence. When 250,000 cells were seeded, a distinct rise of intensity was detected (Fig 3.10).

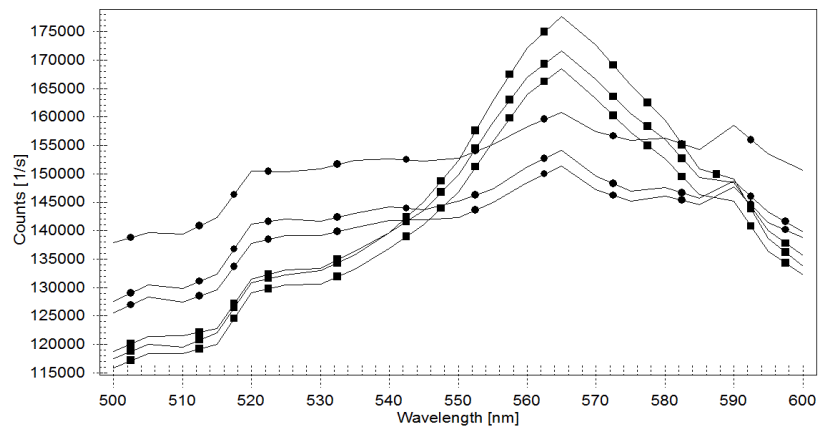


Fig 3.9 Emission scans of untreated (●) and treated (■) (with 16 nM Qdot 565 ITK Carboxyl) samples which were seeded with 50,000 cells. (n=3)

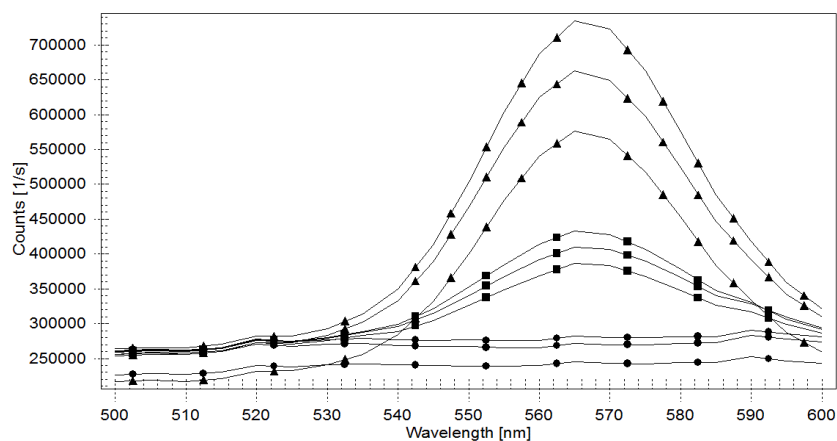


Fig 3.10 Emission scans of untreated (●), treated with 16 nM Qdot 565 ITK Carboxyl (■) and treated with 32 nM Qdot 565 ITK Carboxyl (▲) samples which were seeded with 250,000 cells. (n=3)

3.2.2.2 Calibration Curve Preparation

A calibration curve of fluorescence intensity versus QD solution concentration was used to convert the emission from the cell samples to internalized QD amount. Nine concentrations from 0.005 nM to 0.8 nM were included to the curve. The best fit formula that was derived from the linear regression of the curve was $y = 13040 + 825900x$ which had an r^2 of 0.9941 (Fig 3.11).

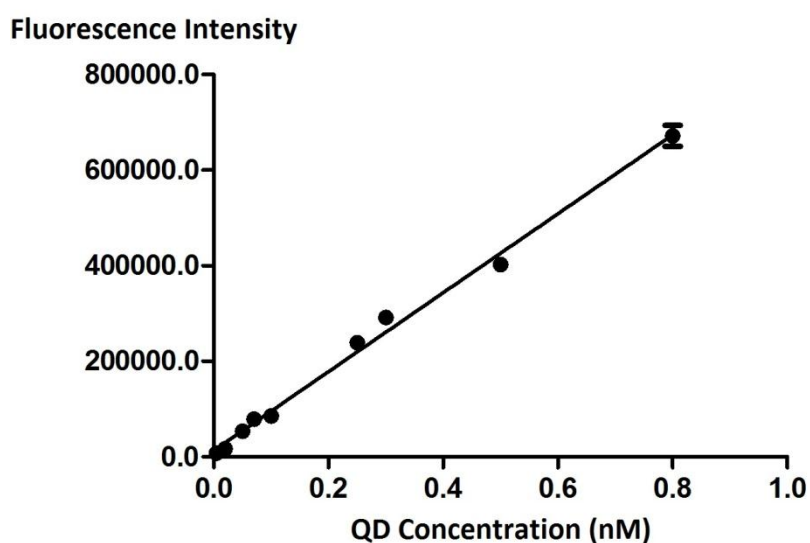


Fig 3.11 Calibration curve for uptake assay of Qdot 565 ITK Carboxyl (n=3)

3.2.2.3 Uptake of Ag₂S Quantum Dots

QD uptake assay was successfully optimized using Qdot 565 ITK quantum dots from Invitrogen. However, when we used the assay to determine Ag₂S QDs uptake, emission signal detection proved to be very difficult due to the optimal photon detection range of the microplate reader. Typical detectors used in plate readers have low sensitivity for the near infra-red photon detection. We scaled-up the assay to include more cells and higher emission from internalized QDs but the instrument still failed to record emission from Ag₂S particles. Currently, we are working on a new assay which will be based on QD absorbance for the quantitative determination of Ag₂S quantum dot uptake.

3.3 Cytotoxicity: Necrosis vs. Apoptosis

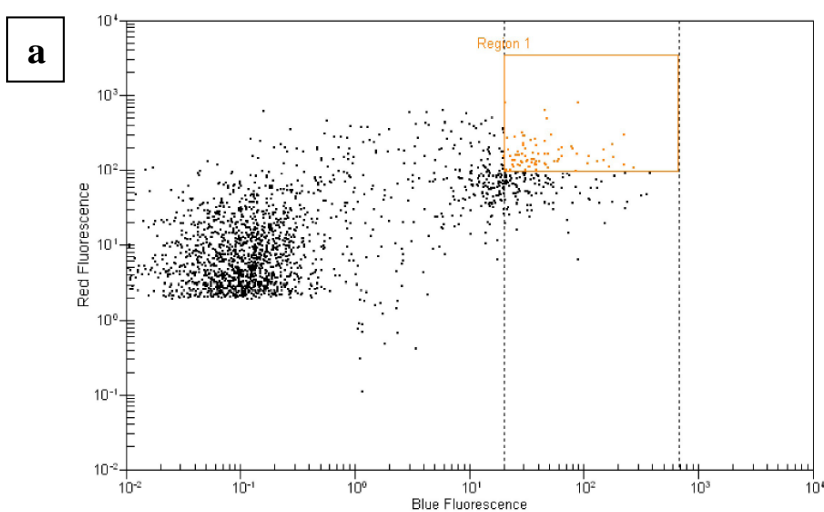
Both necrosis and apoptosis are processes that result with cell death. Even though the outcome is identical, the mechanisms and the causes that induce one or the other are drastically different. Necrosis occurs when physiological conditions of the environment suffer extreme variations. Apoptosis, however, occurs in normal conditions and activated by the cell itself. During apoptosis, ATP and protein production continues and organelles are still working. Cell content is divided into small apoptotic bodies that are surrounded by intact membranes. Those bodies are then phagocytized by either macrophages or adjacent epithelial cells. In contrast, all cell activity is ceased in necrosis. Cell membrane swells and ruptures, releasing cell content into the outer environment.

Ag₂S QDs were evaluated by XTT and proliferation assays in order to determine the cytotoxic effect of the particles. In parallel, we also conducted an apoptosis assay to determine the pathway of the cell death.

The apoptosis ratio of QD treated NIH/3T3 cell population was determined by annexin V based apoptosis assay using Agilent 2100 Bioanalyzer with microfluidic cell chips. Annexin V based apoptosis assay includes two fluorescent dyes which are

called calcein and Cy5. Cy5 is conjugated to Annexin V which binds to phosphatidyl serine (PS). When a cell is apoptotic or necrotic, its PS molecules that reside on the membrane are spread outward. Cy5 conjugated Annexin V binds to these molecules and stains the membrane of apoptotic and necrotic cells red. Calcein is a green fluorescence probe that can only be retained by cells that have intact membranes. Healthy cells and the cells that are in the early stages of the apoptosis have intact membranes. Therefore calcein can stain the cytoplasm of healthy and apoptotic cells. As a result, when the assay is applied, healthy cells are green, necrotic cells are red and apoptotic cells have red membranes while their cytoplasm is green.

Optimization runs were conducted on CdS/Poly(Dimethylamino ethyl methacrylate) QD. It was chosen as a representative QD because it was found to possess high cytotoxic effects when XTT assay was performed. We wanted to see how much of this cytotoxicity is expressed as apoptotic behavior or simple necrosis. NIH/3T3 cells were treated with 25 $\mu\text{g}/\text{mL}$ CdS/Poly(Dimethylamino ethyl methacrylate) for 24 hours. Etoposide, an anti-cancer agent, was used as positive control. Etoposide inhibits the topoisomerase II enzyme. Inhibition prevents re-ligation of the DNA strands during DNA synthesis and promotes apoptosis of the cell (Gordaliza et al, 2004). Etoposide treatment concentration was 0.4 mM for 24 hours.



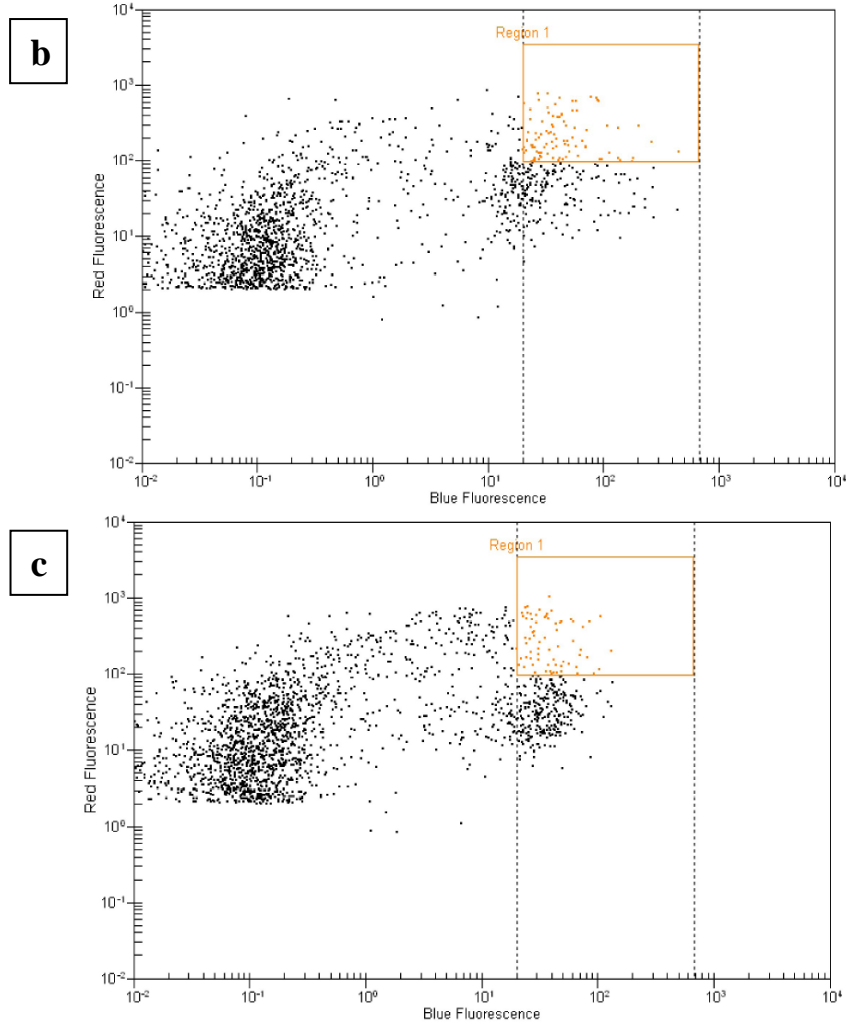
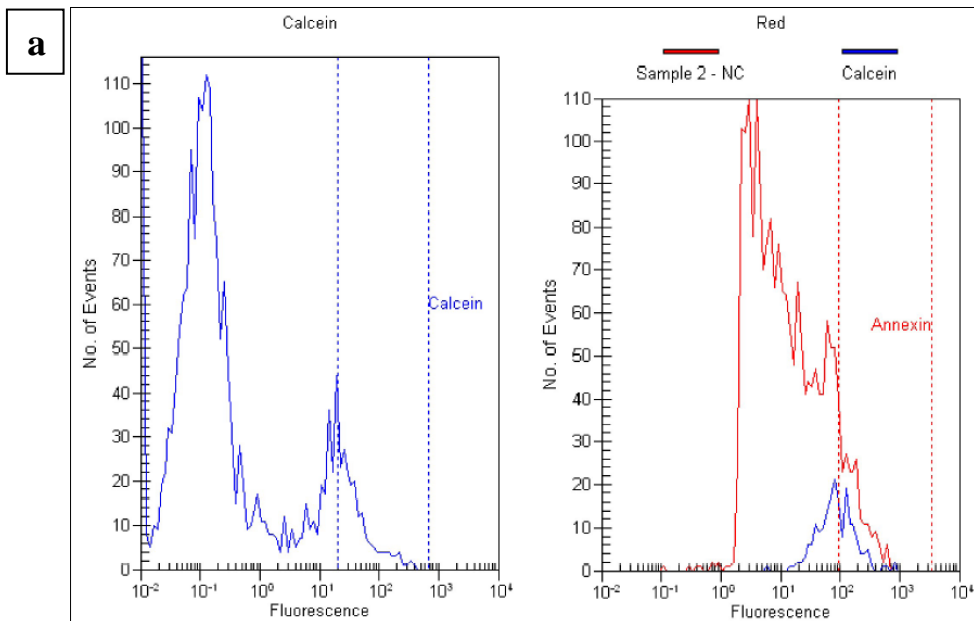


Fig. 3.12 Dot plot of events in terms of fluorescence intensity. a: No treatment, b: etoposide treated, c: QD treated.



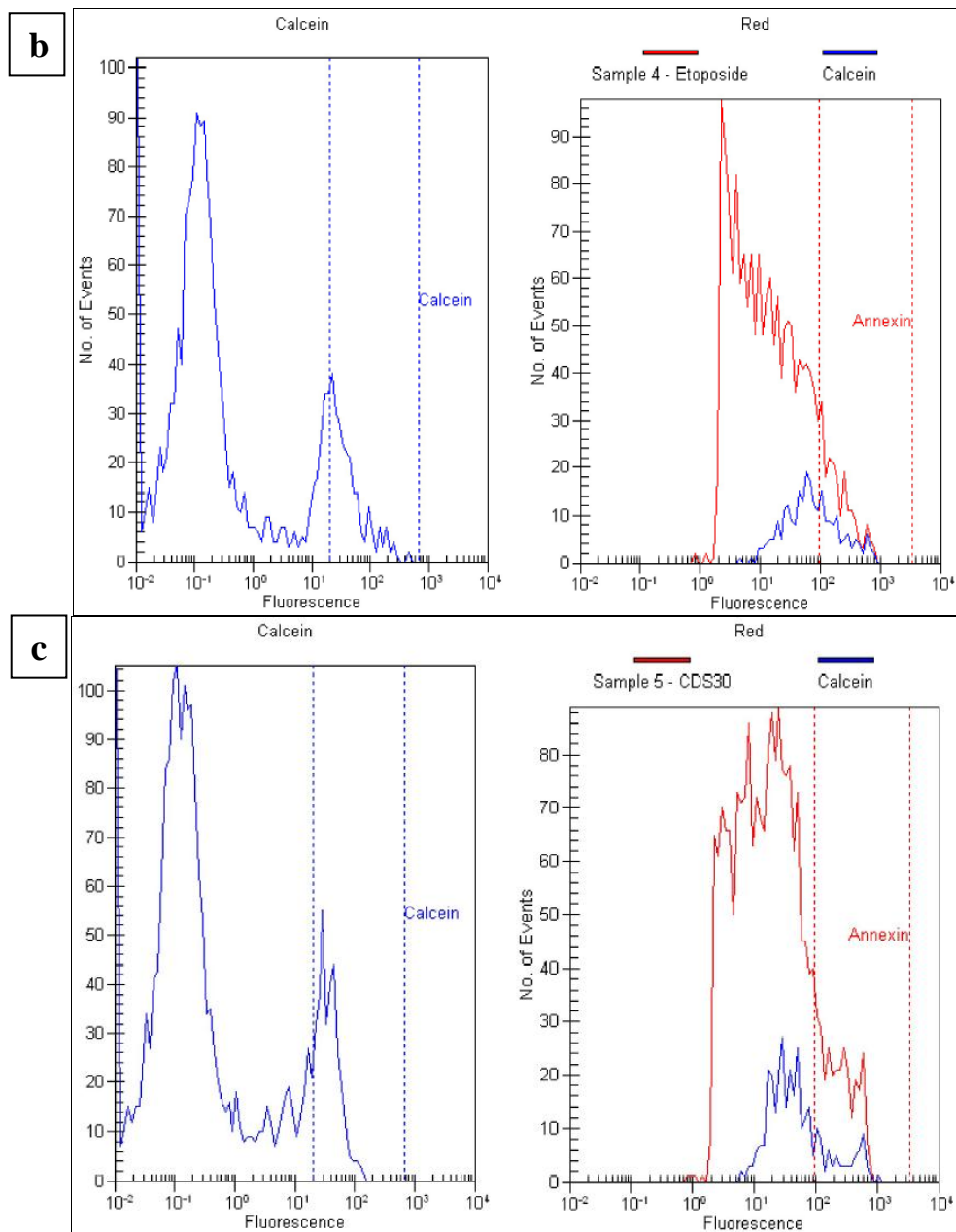


Fig. 3.13 Histogram of events in terms of fluorescence intensity. a: No treatment, b: etoposide treated, c: QD treated.

Bioanalyzer software presents apoptosis assay results with dot plots and histograms. Dot plots (Fig 3.12) show apoptotic cells while histograms (Fig 3.13) give amount of cells that emits a certain dye fluorescence. Regions for apoptosis, calcein and annexin (Cy5) are prefixed by the software and represents the acceptable fluorescence intensity range.

Half of the QD treated sample was found to be necrotic (Table 3.1) which is a result that is in correlation with our XTT findings that showed 50% metabolic activity at this concentration. Low amount of apoptotic cells suggests that CdS/Poly(Dimethylamino ethyl methacrylate) QD does not cause apoptosis but kills the cells by another way. Negative control sample showed unexpected results. It had much more apoptosis and necrosis ratio than the positive control. We suspect that etoposide treatment is so toxic that most of the affected cells are already disintegrated and could not be counted by bioanalyzer. Negative control also showed to have much more apoptotic cells than QD treated sample. This might be a result of the stress caused by the assay application to the healthy cells of negative control. QD treated sample would not be affected as much since most of the cells are already damaged by QD.

The optimization studies of this assay still are ongoing due to problems discussed above. We are searching for a more appropriate apoptotic agent to be used as positive control and the unintended stress on negative control is being investigated. The assay is going to be used on Ag₂S-2MPA after these problems are resolved.

Table 3.1 Percentage of apoptotic, healthy and necrotic cells in untreated, etoposide and QD treated NIH/3T3 cells.

| | Apoptotic (%) | Healthy (%) | Necrotic (%) |
|---------------------|----------------------|---------------------|---------------------|
| Negative control | 27±3 | 34±3 | 39±0 |
| Etoposide treatment | 25±1 | 44±1 | 31±0 |
| QD treatment | 12±1 | 40±6 | 49±8 |

CHAPTER 4

CONCLUSION

This research was conducted in order to investigate the biological application potential of Ag₂S/2-MPA quantum dots. Metabolic activity, cell proliferation, confocal fluorescence microscopy, uptake and apoptosis assays were used for *in vitro* characterization of the nanoparticles. Studies were conducted on NIH/3T3 mouse fibroblast cell line.

XTT determined metabolic activity assay showed that Ag₂S QDs have excellent cytocompatibility even at considerably high concentration (600 µg/mL) in 24 h particle exposure. Metabolic activity and cell proliferation assays show correlation which is a strong support for the biocompatibility of the Ag₂S QDs. It was also shown by confocal laser scanning microscopy that QDs were effectively internalized by the mouse fibroblast cells. Particles displayed punctuated distribution in the cytoplasm which indicates that they are entrapped in the endosomes following cellular internalization by endocytosis.

We also tried to setup an uptake assay for the quantitative determination of QD internalization. This assay was performed on a fluorescence microplate reader. The major difficulty turned out to be the photon detection range of the instrument which is not strong enough in the near infra-red region of the electromagnetic spectrum where Ag₂S QDs emit photons. In future studies, we are planning to measure uptake by absorption instead of emission.

Apoptotic effect of Ag₂S QDs was also investigated in this work. We used an Annexin V based assay on Agilent Bioanalyzer type flow cytometer with microfluidic cell chips for the detection of apoptotic cell fraction following QD and

etoposide (positive control) treatment. During optimization and test studies, similar apoptotic cell numbers were obtained for both negative and positive controls which indicate a critical problem associated with either the instrument or the cell chips used in the assay. Therefore, these experiments will be repeated with new Agilent cell chips and additional positive controls.

In conclusion, we show that owing to its excellent cytocompatibility, effective cellular uptake and NIR emission spectrum which provides cell imaging with minimum cellular autofluorescence, Ag₂S/2-MPA is a promising cellular imaging probe for biological and medical applications.

Ag₂S QDs can also be an ideal probe for *in vivo* studies since near infrared emission can penetrate deeper in tissues. Using appropriate peptide and polymer bioconjugation and functionalization, this promising quantum dot can be further improved for higher cellular uptake, cytosolic delivery in gene and drug delivery applications as well as cell and tissue specific targeting in cancer diagnosis and treatment.

REFERENCES

Agilent Technologies, http://www.chem.agilent.com/Library/applications/59884319_028052.pdf, Last Access Date 07 March 2012

Agilent Technologies, <http://www.chem.agilent.com/library/applications/59887297en.pdf>, Last Access Date 07 March 2012

Agilent Technologies, <http://gcf.pbrc.edu/docs/Agilent/Agilent%20Manual.pdf>, Last Access Date 07 March 2012

Alivisatos A. P., Gu W., Larabell C. (2005). Quantum Dots as Cellular Probes. *Annu. Rev. Biomed. Eng.*, Vol. 7, 55–76

Bailey R. E., Smith A. M., Nie S. (2004). Quantum dots in biology and medicine. *Physica E*, 25, 1–12

Banerjee H. (2010). Special Issue on: "Quantum Dots in Biomedical Research". <http://www.inderscience.com/browse/callpaper.php?callID=1140>, Last Access Date 07 March 2012

Berger M. (2008). Listening to hot quantum dots adds to nanotherapeutic toolbox. <http://www.nanowerk.com/spotlight/spotid=8134.php>, Last Access Date 07 March 2012

Bharali D. J., Dier U., Davis P. J., Mousa S. A. (2009). Tetrac-Conjugated Quantum Dots for Diagnosis and Treatment of Pancreatic Cancer: An In Vitro Evaluation. *Immun., Endoc. & Metab. Agents in Med. Chem.*, 9, 219-223

Biju V., Itoh T., Anas A., Sujith A., Ishikawa M. (2008). Semiconductor quantum dots and metal nanoparticles: syntheses, optical properties, and biological applications. *Anal Bioanal Chem*, 391:2469–2495

Biological Industries, <http://www.bioind.com/htmls/article.aspx?c0=12557&bsp=13275>, Last Access Date 07 March 2012

Chan W. C., Maxwell D. J., Gao X., Bailey R. E., Han M., Nie S. (2002). Luminescent quantum dots for multiplexed biological detection and imaging. *Current Opinion in Biotechnology*, 13:40–46

Cho S. J., Maysinger D., Jain M., Rder B., Hackbarth S., Winnik F. M. (2007). Long-Term Exposure to CdTe Quantum Dots Causes Functional Impairments in Live Cells. *Langmuir*, 23 (4), 1974-1980

Chemical Book, http://www.chemicalbook.com/ChemicalProductProperty_EN_CB3268225.htm, Last Access Date 07 March 2012

Choi A. O., Cho S. J., Desbarats J., Lovric J., Maysinger D. (2007). Quantum dot-induced cell death involves Fas upregulation and lipid peroxidation in human neuroblastoma cells. *Journal of Nanobiotechnology*, 5:1

Claxton N. S., Fellers T. J., Davidson M. W. (2006). Laser scanning confocal microscopy.

Cooper D. R., Dimitrijevic N. M., Nadeau J. L. (2010). Photosensitization of CdSe/ZnS QDs and reliability of assays for reactive oxygen species production. *Nanoscale*, 2, 114–121

CRISP, <http://www.crisp.nus.edu.sg/~research/tutorial/em.htm#mwbands>, Last Access Date 07 March 2012

Das G. K., Chan P. P. Y., Teo A., Loo J. S. C., Anderson J. M., Tan T. T. Y. (2009). In vitro cytotoxicity evaluation of biomedical nanoparticles and their extracts. *Journal of Biomedical Materials Research Part A*, 337-346

Docstoc, <http://www.docstoc.com/docs/44024557/Quick-Start-Guide-Zeiss-LSM-510>, Last Access Date 21 July 2011

El-Sayed A., Futaki S., Harashima H. (2009). Delivery of Macromolecules Using Arginine-Rich Cell-Penetrating Peptides: Ways to Overcome Endosomal Entrapment. *The AAPS Journal*, Vol. 11, No. 1

Fluorescence SpectraViewer, <http://www.invitrogen.com/site/us/en/home/support/Research-Tools/Fluorescence-SpectraViewer.html>, Last Access Date 07 March 2012

Freshney, R. (1987). *Culture of Animal Cells: A Manual of Basic Technique*. 1st Ed. New York: Alan R. Liss, Inc. p 117

Gao X., Cui Y., Levenson R. M., Chung L. W. K., Nie S. (2004). In vivo cancer targeting and imaging with semiconductor quantum dots. *Nature Biotechnology*, Vol. 22, Number 8, 969-976

Glycosan Biosystems, http://www.glycosan.com/peg_science/what_peg.html, Last Access Date 07 March 2012

Han M., Gao X., Su J. Z., Nie S. (2001). Quantum-dot-tagged microbeads for multiplexed optical coding of biomolecules. *Nature Biotechnology*, Vol. 19, 631-635

Hirsch M. P. (1998). Toxicity of silver sulfide-spiked sediments to the freshwater amphipod (*Hyalella azteca*), *Environmental Toxicology and Chemistry*, 17, 601-604.

Hoang M. V., Whelan M. C., Senger D. R. (2004). Rho activity critically and selectively regulates endothelial cell organization during angiogenesis. *PNAS*, Vol. 101, No. 7. 1874–1879

Hughes M. C. (2008). CdSe Quantum Dots. <http://web.michaelchughes.com/Projects/cdse-quantum-dots>, Last Access Date 07 March 2012

Invitrogen, <http://probes.invitrogen.com/media/pis/mp03224.pdf>, Last Access Date 07 March 2012

Invitrogen, <http://probes.invitrogen.com/media/pis/mp07026.pdf>, Last Access Date 07 March 2012

Invitrogen, <http://probes.invitrogen.com/media/pis/mp19020.pdf>, Last Access Date 07 March 2012

Invitrogen, <http://tools.invitrogen.com/content/sfs/manuals/mp36353.pdf>, Last Access Date 07 March 2012

Invitrogen, http://www.invitrogen.com/etc/medialib/en/filelibrary/cell_tissue_ana

lysis/pdfs.Par.7549.File.dat/B-075409-Qdot-brochure-flr.pdf, Last Access Date 07 March 2012

Invitrogen, <http://www.invitrogen.com/site/us/en/home/References/Molecular-Probes-The-Handbook/Indicators-for-Ca2-Mg2-Zn2-and-Other-Metal-Ions/Fluorescent-Indicators-for-Zn2-and-Other-Metal-Ions.html#head5>, Last Access Date 07 March 2012

Invitrogen, <http://www.invitrogen.com/site/us/en/home/References/Molecular-Probes-The-Handbook/ ultrasensitive-Detection-Technology/QDot-Nanocrystal-Technology.html>, Last Access Date 07 March 2012

Jaimeson T., Bakhshi R., Petrova D., Pocock R., Imani M., Seifalian A. M. (2007). Biological applications of quantum dots. *Biomaterials*, 28, 4717–4732

Jaiswal J. K., Simon S. M. (2004). Potentials and pitfalls of fluorescent quantum dots for biological imaging. *TRENDS in Cell Biology*, Vol.14, No.9

Kerr J. F. R., Wyllie A. H., Currie A. R. (1972). Apoptosis: A Basic Biological Phenomenon With Wideranging Implications In Tissue Kinetics. *Br. J. Cancer*, 26, 239

Kobayashi K., Shida R., Hasegawa T., Satoh M., Seko Y., Tohyama C., Kuroda J., Shibata N., Imura N., Himeno S. (2005). Induction of hepatic metallothionein by trivalent cerium: role of interleukin 6. *Biol Pharm Bull.*, 10, 1859-1863

Kondoh M., Araragi S., Sato K., Higashimoto M., Takiguchi M., Sato M. (2002). Cadmium induces apoptosis partly via caspase-9 activation in HL-60 cells. *Toxicology*, 170, 111–117

Lin S., Xie X., Patel M. R., Yang Y. H., Li Z., Cao F., Gheysens O., Zhang Y., Gambhir S. S., Rao J. H., Wu J. C. (2007). Quantum dot imaging for embryonic stem cells. *BMC Biotechnology*, 7: 67

Lovric J., Bazzi H. S., Cuie Y., Fortin G. R. A., Winnik F. M., Maysinger D. (2005). Differences in subcellular distribution and toxicity of green and red emitting CdTe quantum dots. *J Mol Med*, 83: 377–385

Lovric J., Cho S. J., Winnik F. M., Maysinger D. (2005). Unmodified Cadmium Telluride Quantum Dots Induce Reactive Oxygen Species Formation Leading to Multiple Organelle Damage and Cell Death. *Chemistry & Biology*, Vol. 12, 1227–1234

Mahto S. K., Park C., Yoon T. H., Rhee S. W. (2010). Assessment of cytocompatibility of surface-modified CdSe/ZnSe quantum dots for BALB/3T3 fibroblast cells. *Toxicology in Vitro*, Vol. 24, 1070–1077

Malvezzi C. K., Moreira E. G, Vassilieff I., Vassilieff V. S., Cordellini S. (2001). Effect of L-arginine, dimercaptosuccinic acid (DMSA) and the association of L-arginine and DMSA on tissue lead mobilization and blood pressure level in plumbism. *Braz J Med Biol Res.*, Vol. 34(10), 1341-1346.

Meso-2,3-Dimercaptosuccinic Acid (DMSA). (2000). *Alternative Medicine Review*, Vol. 5, Number 3, 264-267, <http://www.thorne.com/altmedrev/.fulltext/5/3/264.pdf>, Last Access Date 07 March 2012

Madelung O. (2004). *Semiconductors: Data Handbook*, Springer, Verlag Berlin Heidelberg Newyork, p. 1528.

Michalet X., Pinaud F. F., Bentolila L. A., Tsay J. M., Doose S., Li J. J., Sundaresan G., Wu A. M., Gambhir S. S., Weiss S. (2005). Quantum Dots for Live Cells, in Vivo Imaging, and Diagnostics. *Science*, Vol. 307, 538-544

Mongillo J. F. (2007) Nanotechnology 101. *Glossary*, (pp. 268). Greenwood Press, London

Nagy A. (2010). *Characterization and Interactions of Nanoparticles in Biological Systems*. Dissertation, The Ohio State University, Ohio, USA

Nan X., Sims P. A., Chen P., Xie X. S. (2005). Observation of Individual Microtubule Motor Steps in Living Cells with Endocytosed Quantum Dots. *J. Phys. Chem. B*, Vol. 109, No. 51, 24220- 24224

Nanoco Technologies, <http://www.nanocotechnologies.com/content/CommercialApplications.aspx>, Last Access Date 07 March 2012

Nanoprint Technologies, http://www.nanoprinttech.com/quantum_dot.html, Last Access Date 07 March 2012

Olympus, <http://www.olympusfluoview.com/theory/fluorophoresintro.html>, Last Access Date 07 March 2012

Qi L., Gao X. Emerging application of quantum dots for drug delivery and therapy. *Expert Opin. Drug Deliv.*, 5(3):263-267

Reed M. A., (1993). Quantum Dots. *Scientific American*, 118-123

Resch-Genger U., Grabolle M., Cavaliere-Jaricot S., Nitschke R., Nann T. (2008). Quantum dots versus organic dyes as fluorescent labels. *Nature Methods*, Vol. 5, No 9

Roche, https://e-labdoc.roche.com/LFR_PublicDocs/ras/11465015001_en_17.pdf, Last Access Date 07 March 2012

Roche, Apoptosis, Cell Death and Cell Proliferation, 3rd ed. https://www.roche-applied-science.com/publications/print_mat/apoptosis_cell_death_cell_poliferati_on_3ed.pdf, Last Access Date 07 March 2012

Rudd C. J., Herschman H. R. (1979). Metallothionein in a human cell line: The response of HeLa cells to cadmium and zinc. *Toxicology and Applied Pharmacology*, Vol. 47, Issue 2, 273-278

Ryman-Rasmussen J. P., Riviere J. E., Monteiro-Riviere N. A. (2007). Surface Coatings Determine Cytotoxicity and Irritation Potential of Quantum Dot Nanoparticles in Epidermal Keratinocytes. *Journal of Investigative Dermatology*, Vol. 127, 143–153.

Ryman-Rasmussen J. P., Riviere J. E., Monteiro-Riviere N. A. (2007). Variables Influencing Interactions of Untargeted Quantum Dot Nanoparticles with Skin Cells and Identification of Biochemical Modulators. *Nano Lett.*, Vol. 7, No. 5

Rzagalinski B. A., Strobl F. S., (2009). Cadmium-containing nanoparticles: Perspectives on pharmacology and toxicology of quantum dots. *Toxicology and Applied Pharmacology*, Vol. 238, 280–288

Scudiero D. A., Shoemaker R. H., Paul K. D., Monks A., Tierney S., Nofziger T. H., Currens M. J., Seniff D., Boyd M. R. (1988). Evaluation of a Soluble Tetrazolium/Formazan Assay for Cell Growth and Drug Sensitivity in Culture Using Human and Other Tumor Cell Lines. *Cancer Research*, 48, 4827-4833

Sevinç E., Ulusoy G., Selçuk F., Akkuzu A., Erdem R., Güngör B., Sayın E., Özen

C., Yağcı Acar F. (2009). Development of Aqueous CdS and CdTe/CdS Quantum Dots with Novel Coatings. Biotech Metu 2009, Turkey, September 27-30

Sigma Aldrich , http://www.sigmaaldrich.com/catalog/ProductDetail.do?D7=0&N5=SEARCH_CONCAT_PNO|BRAND_KEY&N4=W318000|ALDRICH&N25=0&QS=ON&F=SPEC, Last Access Date 07 March 2012

Smith A. M., Duan H., Mohs A. M., Nie S. (2008). Bioconjugated quantum dots for in vivo molecular and cellular imaging. *Advanced Drug Delivery Reviews*, 60, 1226–1240

Smith A. M., Gao X., Nie S. (2004). Quantum Dot Nanocrystals for In Vivo Molecular and Cellular Imaging. *Photochemistry and Photobiology*, 80: 377-385

Su Y., Hub M., Fan C., He Y., Li Q., Li W., Wang L., Shen P., Huang Q. (2010). The cytotoxicity of CdTe quantum dots and the relative contributions from released cadmium ions and nanoparticle properties. *Biomaterials*, Vol. 31, 4829-4834

Suresh A. K., Doktycz M. J., Wang W., Moon J. W., Gu B., Meyer H. M., 3rd, Hensley D. K., Allison D. P., Phelps T. J. and Pelletier D. A. (2011). Monodispersed biocompatible silver sulfide nanoparticles: facile extracellular biosynthesis using the gamma-proteobacterium, *Shewanella oneidensis*. *Acta Biomater*, 7, 4253-4258

Tirosh O., Barenholz Y., Katzhendler J., Prieval A. (1998). Hydration of Polyethylene Glycol-Grafted Liposomes. *Biophysical Journal*, Vol. 74, 1371–1379

Vashist S. K., Tewari R., Bajpai R. P., Bharadwaj L. M., Raiteri R. (2006) Review of Quantum Dot Technologies for Cancer Detection and Treatment. *AZojono Journal on Nanotechnology Online*, Vol. 2, 1-14

Yagci Acar H., Kas R., Yurtsever E., Ozen C., Lieberwirth I. (2009). Emergence of 2MPA as an Effective Coating for Highly Stable and Luminescent Quantum Dots. *J. Phys. Chem. C*, 113, 10005–10012

Yarema M., Pichler S., Sytnyk M., Seyrkammer R., Lechner R. T., Fritz-Popovski G., Jarzab D., Szendrei K., Resel R., Korovyanko O., Loi M. A., Paris O., Hesser G. N. and Heiss W. (2011). Infrared Emitting and Photoconducting Colloidal Silver Chalcogenide Nanocrystal Quantum Dots from a Silylamide-Promoted Synthesis *ACS Nano*, 5, 3758-3765

Zhang Z., Lei Y., Dhaliwal A., Ng Q. K., Du J., Yan M., Lu Y., Segura T. (2011). Protein-Polymer Nanoparticles for Nonviral Gene Delivery. *Biomacromolecules* 12, 1006–1014

Zhang L. W., Monteiro - Riviere N. A. (2009). Mechanisms of Quantum Dot Nanoparticle Cellular Uptake. *Toxicological Sciences*, 110(1), 138–155

Zhou M., Ghosh I. (2007). Current Trends in Peptide Science Quantum Dots and Peptides: A Bright Future Together. *Wiley Periodicals, Inc. Biopolymers (Pept Sci)*, 88: 325–339

APPENDIX A

MEDIUM SPECIFICATIONS

Table A.1 MEM liquid medium with Earle's salts, NaHCO₃ and stable glutamine

| Compound | Concentration (mg/L) | Compound | Concentration (mg/L) |
|--|-------------------------|-------------------|-------------------------|
| L-arginine·HCl | 126 | L-tyrosine | 36 |
| L-cystine | 24 | L-valine | 46 |
| L-glutamine | 292 | Folic acid | 1 |
| L-histidine·HCl·H ₂ O | 42 | Cholin chloride | 1 |
| L-isoleucine | 52 | Nicotinamide | 1 |
| L-leucine | 52 | D-Ca-pantothenate | 1 |
| L-lysine·HCl | 73 | Pyridoxal·HCl | 1 |
| L-methionine | 15 | Thiamine x HCl | 1 |
| L-phenylalanine | 32 | Riboflavin | 0.1 |
| L-threonine | 48 | Myo-inositol | 2 |
| L-tryptophane | 10 | NaCl | 6800 |
| KCl | 400 | CaCl ₂ | 200 |
| MgSO ₄ ·7H ₂ O | 200 | D-glucose | 1000 |
| NaH ₂ PO ₄ ·H ₂ O | 140 | Phenol red | 10 |
| NaHCO ₃ | 2200 | | |

Table A.2 DMEM liquid medium with stable glutamine, 3.7 g/L NaHCO₃, 1.0 g/L D-glucose

| Compound | Concentration (mg/L) | Compound | Concentration (mg/L) |
|--|----------------------|-------------------|----------------------|
| NaCl | 6400 | L-methionine | 30 |
| KCl | 400 | L-phenylalanine | 66 |
| CaCl ₂ | 200 | L-threonine | 95 |
| MgSO ₄ ·7H ₂ O | 200 | L-tryptophane | 16 |
| NaH ₂ PO ₄ | 124 | L-tyrosine | 72 |
| D-glucose | 1000 | L-valine | 94 |
| Fe(NO ₃) ₃ ·9H ₂ O | 0.1 | Glycine | 30 |
| Na-pyruvate | 110 | L-serine | 42 |
| Phenol red | 15 | Cholin chloride | 4 |
| NaHCO ₃ | 3700 | Folic acid | 4 |
| L-arginine·HCl | 84 | Myo-inositol | 7.2 |
| L-cystine | 48 | Nicotinamide | 4 |
| L-glutamine | 580 | D-Ca-pantothenate | 4 |
| L-histidine·HCl·H ₂ O | 42 | Pyridoxal·HCl | 4 |
| L-isoleucine | 105 | Riboflavin | 0.4 |
| L-leucine | 105 | Thiamine·HCl | 4 |
| L-lysine·HCl | 146 | | |

APPENDIX B

SOLUTIONS

50X PB Stock Solution

43.5 g K_2HPO_4

33.5 g KH_2PO_4

Dissolved in dH_2O and pH was adjusted to the 6.7 with NaOH. Volume is completed to the 500 mL with dH_2O . Filtered through 47 mm filter (Sigma- Aldrich, USA).

10X PBS Solution

200 mL 50X PB stock solution

1800 mL dH_2O

87 g NaCl

pH was adjusted to the 7.2 with NaOH and volume completed to the 1 liter with dH_2O . Filtered through 47 mm filter and autoclaved at $121^{\circ}C$ for 20 min.

1X PBS Solution

20 mL 50X PB stock solution

180 mL dH_2O

8.7 g NaCl

pH was adjusted to the 7.2 with NaOH and volume completed to the 1 liter with dH_2O . Filtered through 47 mm filter and autoclaved at $121^{\circ}C$ for 20 min.

4% Paraformaldehyde

0.4 g paraformaldehyde

7 mL dH₂O

1 mL 10X PBS

pH was adjusted with HCl to 7.4 and volume was completed to the 10 mL with dH₂O.